Optical chemical sensors based on hybrid organic-inorganic sol-gel nanoreactors

Thu-Hoa Tran-Thi, Romain V.H. Dagnelie, Sabine Crunaire, Lionel Nicole

Optical chemical sensors based on hybrid organic–inorganic sol–gel nanoreactors

Thu-Hoa Tran-Thi,[a] Romain Dagnelie,[a] Sabine Crunaire[a] and Lionel Nicole[bc]

[a]CEA, IRAMIS/SPAM/Laboratoire Francis Perrin, URA 2453, Centre d'Etudes de Saclay, F-91191 Gif-sur-Yvette Cedex, France. E-mail: thu-hoa.tran-thi@cea.fr; Fax: 33-1-69081213; Tel: 33-1-69084933

[b]UPMC Univ Paris 06, UMR 7574, Laboratoire Chimie de la Matière Condensée de Paris, F-75005, Paris, France

[c]CNRS, UMR 7574, Laboratoire Chimie de la Matie`re Condensée de Paris, F-75005, Paris, France. E-mail: lionel.nicole@upmc.fr; Fax: 33-1-44271504; Tel: 33-1-44271529

Sol–gel porous materials with tailored or nanostructured cavities have been increasingly used as nanoreactors for the enhancement of reactions between entrapped chemical reactants. The domains of applications issued from these designs and engineering are extremely wide. This *tutorial review* will focus on one of these domains, in particular on optical chemical sensors, which are the subject of extensive research and development in environment, industry and health.

1. Introduction

Recent developments in the field of optical chemical sensors mostly involve improvement of sensing platforms (optical fibres, planar waveguides, microfluidic devices), miniaturisation of light sources and detectors, development of sophisticated detection techniques (for example, direct luminescence intensity detection is progressively replaced by lifetime-based measurements involving sophisticated phase-based techniques)[1] rather than new sensing materials. However, the discovery of periodically organised mesoporous materials (POMMs) and the application of molecular imprinting strategies to sol–gel materials offer new matrices with improved properties.

The sol–gel chemistry also allows the tailoring of the pore size, and narrow pore distributions can be obtained by varying the synthesis parameters, such as the nature of the precursors of polymerisation, the ratio of the concentrations of the precursor, organic solvent and water and the final pH of the sol. Moreover, some materials can display very ordered nanostructures with uniform pore sizes or hierarchical structures with microscopic (<2 nm) and mesoscopic (2–50 nm) domains. The utility of such tailored or organized media and the possibility of reproducing liquid phase chemical reactions in these confined nanoreactors are here shown with regard to their potential as sensitive matrices or layers of chemical sensors for the detection of gaseous and ionic analytes. To illustrate the potential of the porous materials and the importance of the chemical reactivity at gas–solid or liquid–solid interfaces, a few examples of innovative optical chemical sensors will be given with a particular emphasis on the relationship between the design of the material, the transduction mode coupled with the microfluidic system and the targeted application.

The present article is divided into four main sections. After the Introduction, a brief description of the available optical transduction modes will be given followed by a section on the rational design of sol–gel materials where the strategies of synthesis and doping are shortly reviewed. Then, a few examples of innovative chemical sensors for the detection of gaseous and ionic compounds will be detailed before we conclude with the future prospectives.

2. Optical transduction modes

Absorption and fluorescence

Standard absorbance and fluorescence of reactants entrapped in sol–gel matrices remain the most popular detection modes, over the UV, visible and near-IR domain. A typical embodiment comprises a sensitive material (monolithic xerogel or film deposited on a transparent substrate) that changes colour upon interaction or reaction with the targeted analyte. For absorbance measurements, the probe light can be either directly transmitted through the sensitive material or reflected on the surface of a thin film and collected *via* a photomultiplier or a diode array. With optical fibers to improve the light collection, many configurations were proposed in the literature and reviewed by McDonagh *et al.*[1] Briefly, the sol–gel layer can be deposited on the inner surface of the fiber (doped cladding), thus enhancing the absorbance of light along the pathway, or as an end face at the end of the fiber. Bifurcated fiber bundles can also be used to deliver the excitation photons with one fiber and collect the fluorescence photons with the other. Many pH sensors with pH sensitive dyes entrapped in a sol–gel matrix were designed as such.[2] With the aim of miniaturising and lowering the price of the detection system, innovative planar waveguides based on the propagation of the light within the substrate on which the sol–gel layer is coated were exploited to detect various analytes in the gas[3] as well as liquid phase.

Recent advances in luminescence-based sensors involve the reagent lifetime measurement which allows the problems usually encountered with fluorescence intensity measurements such as fluctuation of the excitation source, leaching or photobleaching of the fluorescent product to be overcome. The long lifetime requested for the fluorophore (lifetime > 1 μs) is limiting since very few probes such as ruthenium complexes or porphyrin macrocycles were found to be suitable. The

lifetime can be directly measured *via* single photon counting technique or with intensified CCD camera. Such systems were used to measure pH or detect O_2.[1,2] These methods which require complex and costly apparatus are nowadays replaced by phase fluorimetry, a technique suitable for low-cost sensors since it allows the use of LED sources and photodiode detectors. In that case, the excitation source is modulated in frequency as well as the emitted fluorescence, with a phase shift of the latter signal related to the luminescence lifetime.

In response to the lack of long-lived and sensitive fluorophores, the strategy of dual-lifetime referencing (DLR) making use of two indicators immobilized in the same matrix was developed by Huber *et al.*[4] The indicator with the short lifetime is analyte sensitive while the reference indicator is analyte insensitive and long-lived. Changes in the intensity ratio of the two fluorophores due to the reaction of the short-lived species with the analyte are reflected as changes in the measured phase angle.

Modified DLR method was applied for the simultaneous detection of O_2 and CO_2.[5,6] In this scheme, the two indicators display absorption and fluorescence bands which overlap and they can be excited with the same light source. The analytical information is here obtained by the measurement of the phase shifts at two modulation frequencies (see section 4.2).

Another approach is to combine the lifetime measurements with fluorescence resonance energy transfer (FRET). This method allows the combination of a long lived donor-fluorophore and a dye whose absorption band overlaps the fluorescence band of the donor. Here, the colour change of the dye is converted into a lifetime information. pH indicators coupled with long lived excited states of ruthenium polypyridyl complexes were used to detect CO_2 over a wide range of concentrations (0–100% CO_2, see section 4.2).[7]

3. Strategies of synthesis and doping of sol–gel materials

3.1 Mesostructured materials

The discovery in the 1990s of a new class of materials which combines sol–gel chemistry and organic template approach has been a significant breakthrough for advanced materials research.[8,9] These periodically organised mesoporous materials (POMMs) involve the condensation of inorganic or hybrid precursors around micellar and lyotropic liquid-crystal phases. Briefly, two main mesostructuration processes leading to POMMs have been identified.[8] The first is the liquid crystal templating mechanism in which the inorganic phase condenses around a stable surfactant mesophase. The second is the cooperative self-assembly mechanism, in which surfactant molecules and inorganic species combine in a first step to form an intermediate hybrid mesophase. However, depending on the critical chemical and processing parameters, a combined effect of both mechanisms could be involved in the elaboration of such meso-organised hybrid phases.

Since their discovery, an increasing amount of POMMs presenting very diverse inorganic or hybrid chemical compositions (oxides, carbons, chalcogenides, semi-conductors, *etc*...) involving various organic templates (ionic and non ionic surfactants, amphiphilic block copolymers, biopolymers, *etc*...), shaped as powders, monoliths, thin films, membranes or fibers have appeared[8] and found applications in a wide range of domains (separation techniques, sensors, catalysis, micro-optics and photonic devices, photovoltaic and fuel cells, microelectronics, *etc*...). It is worth mentioning that mainly silica-based POMMs are involved in the field of optical chemical sensors.

The main difference with conventional sol–gel materials is the presence of an ordered nanometric array of perfectly calibrated pores (once the surfactants are removed) surrounded by an inorganic or hybrid network. They then display a large interconnected and opened porosity, a high surface area, a narrow pore size distribution, a tunable pore dimension and shape (cylindrical, spherical, ellipsoidal, *etc*...). These textural characteristics should overcome the main limitation of sol–gel materials in the field of chemical sensors *i.e.* a slow diffusion of ions and large molecules into sol–gel matrices.[2] Moreover, chemical modifications of the network surface could be easily achieved through adsorption of organic compounds or chemical coupling of organo-metallic/organo-silanes species. Investigations on POMMs as sensors matrices demonstrated that they favour analyte diffusion and improve both sensitivity and response time compared to conventional sol–gel materials (*i.e.* materials synthesised without templates).[10–12] However, such an opened porosity could induce an important leaching of sensitive molecules especially for sensor devices working in the liquid phase. The main strategy to overcome this drawback implies the covalent grafting of sensitive probes. In this sense, two main routes have been developed involving different stages of POMM formation: the ''one-pot'' synthesis and the post-functionalisation. The first one, *i.e.* ''one-pot'' synthesis, involves a co-condensation step between a functional organosilane, with an inorganic precursor (typically TEOS or TMOS) in the presence of templates. In this case the mesostructuration process and functionalisation take place at the same time. In the second one, *i.e.* post-functionalisation, chemical modifications come off once mesostructuration and calcination steps are achieved, *via* solution impregnation (reflux in toluene), through chemical bonds with silanol covering the pore surface. Post-functionalisation was mainly exploited to modify properties of mesoporous powders and monoliths (for an overview of functionalisation of mesoporous powders, see the review in ref. 13), while ''one-pot'' synthesis was the usual route leading to functional POMMs shaped as thin films (POMTFs).[14,15]

The co-condensation route generally leads to a more homogeneous distribution of organic functionalities into mesoporous matrices with a high control of the stoichiometry.[13] The final materials exhibit a small decrease of the pore sizes and pore volume only. However, the synthesis could be more delicate due to different effects of organic functions on mesostructuration process especially for POMTFs.[15] On the other hand, post-functionalisation overcomes some difficulties related to the ''one-pot'' synthesis. Since mesostructuration process and grafting are two distinct steps, the influence of organic functionalities is seriously restricted. Moreover, the thermal treatment at high temperature ($\sim$500 °C) allowed by the absence of organic functionalities favors more stable

matrices. However, this method often leads to a quite low loading, an inhomogeneous distribution of the functional groups inside matrices, a decrease of the pore volume and even, in extreme cases, a complete closure of the pores.

Although the vast majority of functionalised POMMs are obtained *via* "one-pot" and post-functionalization pathways, combined routes have been investigated. This combined approach could occur when organosilanes are not commercially available. Instead of synthesising the desired organosilanes before materials synthesis, some authors elaborated hybrid POMMs through a co-condensation or post-functionalization procedure with an organosilane bearing a reactive functional group (typically amino, thiol, isocyanato, and iodo groups). After removal of the surfactant, the post-modification involving the reactive function anchored into POMMs and the organic molecule (for example: fluorescein, rhodamine B, squaraine, azo diazopyrene, anthracene derivatives) could take place. This combined approach presents both the advantages of avoiding the synthesis of organosilanes that are too intricate and limiting the influence of organosilanes (often bulky) on the mesostructuration process.

An alternative way of covalent grafting involves electrostatic interactions (ion pairing approach) and/or hydrophilic/hydrophobic interactions of sensitive molecules with POMMs surface. Three main strategies depending on the chemical nature of sensitive probes were investigated.

With ionic chromophores, a covalent post-grafting of organosilanes of opposite charge is first achieved followed by impregnation/washing cycles of ionic probes solution.[11] The great interests of this alternative way are the commercial availability of charged organosilanes bearing carboxylate, phosphonate, sulfonate or quaternary ammonium functions (see for example the silane coupling agents catalogue at http://www.gelest.com/) and the resulting strong ion-pair interactions which usually limit considerably leaching process of the adsorbed probe.

Hydrophilic chromophores could also be chemically modified with the addition of a long hydrophobic alkyl chain.[11] A simple impregnation step of POMMs with a solution containing such modified chromophores allows their direct immobilisation inside the POMMs' pores. Retention of chromophores is ensured by (i) short-range electrostatic interactions (*i.e.* van der Waals and hydrogen-bonding interactions) between the hydroxy groups on the POMM's surface and heteroatoms of the hydrophilic part of probes and (ii) hydrophobicity of alkyl chain, both of them limiting probes leaching in aqueous solutions. An original approach also based on chemical modification of chromophores has been recently reported.[16] Organic probes were first functionalised with 1,10-dibromodecane species and a subsequent treatment with a trimethylamine compound led to the formation of a sensitive quaternary ammonium surfactant which is

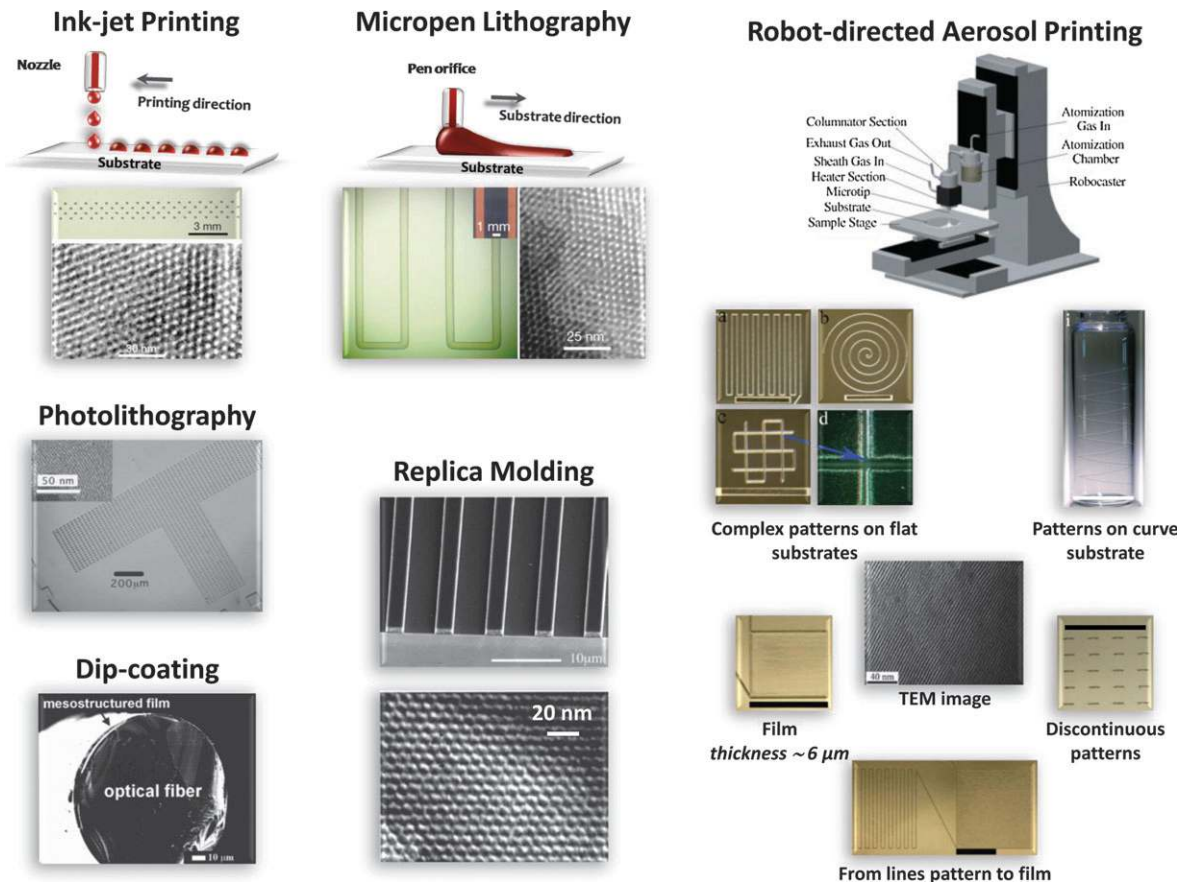

Fig. 1 Various mesostructured silica patterns (photographs and TEM pictures) obtained *via* industrial chemical solution deposition techniques.[20,21,23] Ink-jet printing and micropen lithography: Copyright © 2000 Nature publishing group. Soft lithography: Copyright © 2001 Science. Robot-directed aerosol printing: Copyright © 2008 Wiley-VCH.

used in POMMs synthesis. Here again, leaching of sensitive amphiphilic probes in aqueous solution is limited while sensitivity and response time are greatly improved.

The last approach is mainly based on hydrophobic/hydrophilic balance of both sensitive probes and POMMs and concerns hydrophobic chromophores. In contrast to conventional sol–gel materials, POMMs are characterised by a periodically organised organic/inorganic nanophase separation. Thus, at the nanoscale, structure of POMMs can be divided into three main regions: (i) the silica framework, (ii) a *hydrophilic* aqueous interface formed by the polar heads of surfactant and the inorganic network and (iii) the organic region composed of the hydrophobic core of micelles. A general trend based on the concept "like dissolves like" concerning the placement of guest molecules is as follows: solubilisation of lipophilic molecules occurs in the hydrophobic micelle core and the location of hydrophilic molecules either in the aqueous interface or in the framework (the last case implying a "one-pot" synthesis). Then, hydrophobic chromophores could be easily dissolved in the organic part of micelles in a large amount without both aggregation and mobility constraint (on the contrary to conventional sol–gel matrices) and with a low leaching due to the protective micellar environment.[17] This dye solubilisation could be achieved either during the "one-pot" synthesis or after a first surfactant immobilisation in calcined POMMs.

However depending on the systems studied, these strategies could overlap. For example Eriochrome cyanine R, an hydrophilic dye bearing a sulfonate group, was successfully immobilised, following a "one-pot" procedure, in POMTFs due to ion-pair interactions with the quaternary ammonium head groups of surfactant.[18] The location of the ECR dye at the aqueous interface allowed an easy detection of copper ions while the strong ion-pair interactions hindered dye leaching.

Despite interesting demonstrations of the sensing properties of hydrid POMMs shaped as powders and monoliths that will be presented in the next section, thin films show the most suitable morphology for sensing platforms such as optical fibres and planar waveguides. This is mainly due to their high optical transparency in the UV-visible range, their handling abilities and their versatility of processing (coatings on various substrates such glasses, silicon wafers, plastics, metals by numerous deposition techniques). The following paragraphs will be dedicated to periodically organised mesoporous thin films (POMTFs).

POMTFs are preferentially synthesised *via* the "evaporation induced self assembly" (EISA) approach[17,19] which is the most suitable route for sensing devices. This approach is highly compatible with chemical solution deposition techniques commonly used in industry (dip-, spin-, spray-coatings, ink-jet printing, micropen lithography, aerosol-assisted writing processes, replica molding...) leading to various patterns (Fig. 1).[20–23] The process is fast since mesostructuration could take place, in the case of silica-based materials, within a few minutes (in contrast to powders obtained *via* the precipitation route which takes 24–48 hours). It leads to thin films of good optical quality, transparent in the UV-visible range, highly reproducible with a perfect control of the stoichiometry. Another advantage of EISA is the easiness of the control quality since a 5 minute XRD experiment at low angles, just after the coating step, is sufficient to know if the thin films are mesostructured or not. Obviously, this first XRD-based check has to be completed by several other techniques (transmission electron microscopy, environmental ellipsometric porosimetry for example) in order to fully characterise the POMTFs.[15]

The EISA process could be divided into four steps.[15,19,24] It first implies the elaboration of an isotropic dilute solution containing mainly inorganic (or hybrid) precursors, solvents, catalysts and surfactants (Fig. 2). In a second step during the coating process, the fast evaporation of volatile species (typically ethanol, HCl, H_2O) triggers the self-assembly process by progressively concentrating the system in inorganic precursors and surfactant. In due time, the concentration in surfactant reaches the equivalent of the critical micellar concentration for the system, and then micelles start to form, surrounded by the inorganic precursors. Depending on the processing conditions (*i.e.* water and solvent relative pressures, temperature) the micelles could self-organize on a large scale leading to a liquid-crystalline phase before the extended condensation of inorganic species will lock the system. This step is known as the tunable steady state (TSS). The third step is dedicated to the removal of the surfactant, the stiffening of the inorganic network and eventually the crystallization of the inorganic walls. It is interesting to point out at this stage that the stoichiometry of the final thin film is equal to the composition (in non-volatile species) of the initial solution. Another interesting feature of the EISA process is the embedding of nanoparticles in the POMTFs which is achieved without aggregation. This could be achieved by a simple addition of a colloidal dispersion of particles into the

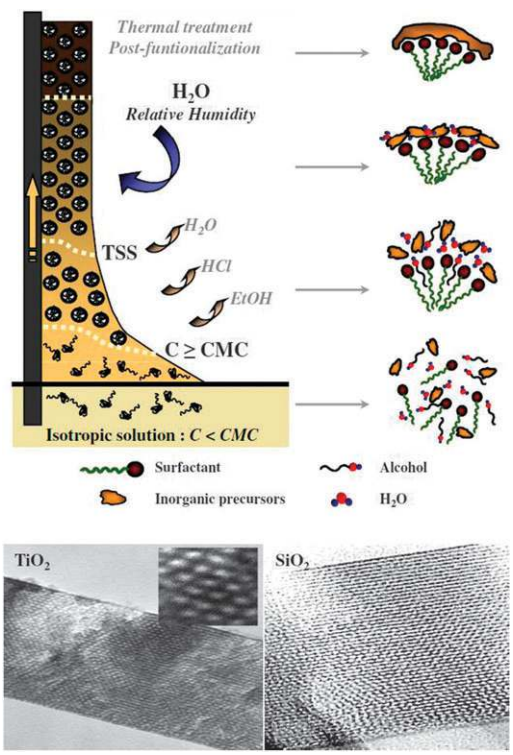

Fig. 2 A schematic representation of the EISA mechanism *via* dip-coating. TEM images of titania and silica POMTFs.

starting sol (keeping in mind that the starting solution should remain isotropic).

In order to fully exploit the potential of functionalised POMTFs, each step of the EISA process has to be carefully controlled since sensitive probes could have serious influences on the mesostructuration.

For example, the addition of functional organosilanes in the starting sol could modify and in some extent hinder the mesostructuration process. With silylated probes poorly soluble or insoluble in the alcoholic sol, segregation or aggregation could take place. This phenomenon may be due to an insufficient hydrolysis of the organosilane precursor, resulting in hydrophobic species. In some cases, the precursor could be insoluble regardless of the hydrolysis rate. To overcome these problems, the replacement of a part of ethanol by tetrahydrofuran is the widespread solution due to both its high solubilisation abilities and physico-chemical properties close to those of ethanol. It is also important to point out that the amount of cosolvent in the initial sol should be adapted to avoid phase separation during the evaporation step (higher than the quantity necessary to solubilise the organosilane especially when its boiling point is lower than that of ethanol).

Another common difficulty involves organosilanes, which could modify the hydrolysis-condensation kinetics of silica species. Organosilanes bearing a basic function, typically an amino group, which are commonly used as coupling agents, catalyse hydrolysis and condensation reactions of silica precursors and can yield the fast gelation of the sol. Acidic conditions in EISA are important to make thin films presenting high optical quality. To avoid basic catalysis of silica species, amino groups are first usually neutralised with a strong acid prior to the addition of the silica precursor. A subsequent treatment of thin films with ammonia could allow the recovery of the amino group.

The third classical issue is encountered for POMTFs presenting a high loading of organosilanes. Above 20% of organosilanes in POMTFs, thin films are usually poorly organised. A modified procedure of the co-condensation route has been successfully tested. On the contrary to the co-condensation which implies the mixing of all the components simultaneously in the initial solution, the ''delayed'' procedure consists in the addition of organosilanes just prior the sol deposition. However, this delayed procedure modifies the main parameters of EISA as surfactant/inorganic precursor molar ratio and the optimum relative humidity within the dip-coater.

During the ''self-assembly induced by evaporation'' step, various modifications of the mesostructure could be observed, depending on the nature of the functional group (hydrophobic, hydrophilic, ionic, aromatic, polar, apolar) and the length of the organic chain between the functional moiety and the anchoring group ($-Si(OR)_3$). These modifications could be simple variations of the lattice parameters, phase transitions, formation of a mesophase for a (very) low molar ratio of surfactant/silica or progressive destructuration of the mesophase. For example, starting with a cubic phase, the incorporation of an increasing amount of bulky hydrophobic sensitive dyes (silylated or not) induces phase transitions from the cubic phase (*Pm*3*n*) to the 2D-hexagonal phase (*p*6*m*) and finally to the lamellar phase. Since tridimensional mesophases (cubic or 3D-hexagonal) are much more stable in aqueous environment than the most often obtained 2D-hexagonal structure,[25] one could favour such 3D mesophases for sensing applications in the liquid phase. This could be achieved by preferentially selecting the combined approach (described previously) for functionalising POMTFs.

The thermal treatment (temperature/duration) has to be adapted to hybrid mesostructured thin films, *i.e.* stiffening the inorganic network without decomposing functional organosilanes. Heating at moderate temperature (strengthening of the framework) followed by a washing step (extraction of surfactant) is usually performed.

In term of matrices stability, which is a crucial parameter in sensors field, POMTFs made with triblock copolymers (Pluronic®) are less stable than those prepared with ionic surfactants.[25] Several strategies have been employed to increase the stability of thin films such as post-densification in the presence of TEOS/TMOS vapour, hydrophobisation with hexamethyldisilazane or ''one-pot'' incorporation of transition metal oxide precursors (such as Zr or Ti oxide precursors).[26]

3.2 Molecular imprinted thin films

The strategy of molecular recognition *via* electrostatic, π-stacking, dipole–dipole or H-bond interactions, was known long ago and was used in molecular imprinted polymers (MIP) for the production of selective sensors or specific adsorbents.[27] Since the past decade, its application to sol–gel materials based sensors became very popular.[28–30]

Once the nature of the template molecules and the targeted analytes is determined, the imprinting process implies two steps, the incorporation of the template in the polymer network and its removal. Various approaches were developed depending on the nature of the analytes. They are summarised in Fig. 3.

With the non-covalent imprinting method (Fig. 3A), in addition to the template molecule, a functional metal alkoxide precursor and a functional monomer which could co-polymerise with the former are needed. The functional monomer would end lying on the surface of the pores and interacting with the template. The nature of the metal alcoxide precursor and solvent must be selected to yield a solid porous matrix with pores large enough to easily remove the templates molecules. This strategy is however limited to templates or targeted molecules which possess functional groups.

The covalent molecular imprinting method (Fig. 3B), which exploits reversible covalent bonds between binding site monomers and a template molecule, allows to overcome this limitation. In this case, the template molecule is functionalized for polymerization and is bound to the pore cavity. The covalent bonds are then chemically cleaved to release the template, and the remaining functional sites are derivatized to bind the target molecule.

Another approach proposed by Whitcombe *et al.*[31] implies the use of a sacrificial spacer, whose nature is similar to the targeted analyte (Fig. 3C). To detect cholesterol *i.e.*, the authors used cholesteryl(4-vinyl)phenylcarbonate ester as

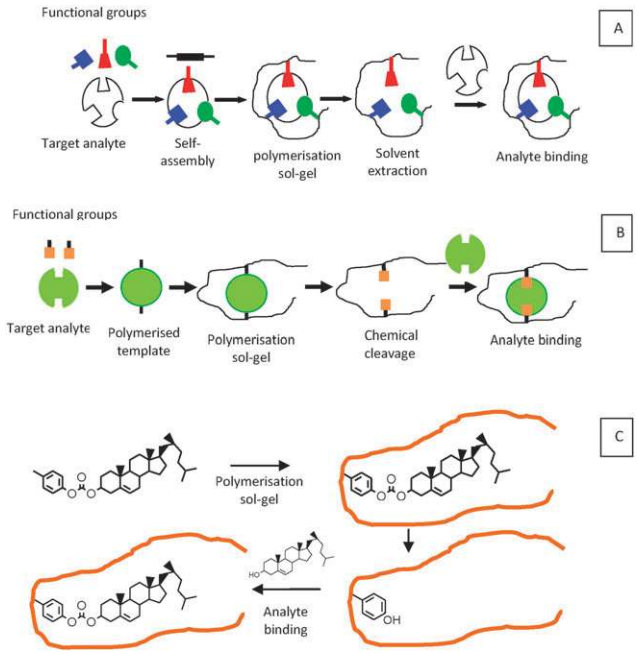

Fig. 3 A schematic view of the MIP fabrication strategies. A: non-covalent imprinting, B: covalent imprinting, C: sacrificial spacer imprinting with the example of cholesterol detection.[29]

functional monomer. The ester bond is then chemically cleaved and the remaining phenolic residue bound to the pore surface can interact with cholesterol *via* hydrogen bond. However, this strategy has some drawbacks, as the pore size must be large enough to allow the removal of cholesterol and many interferent molecules with a small size can diffuse rapidly in the pore and interact *via* H-bond with the phenol residue.

One of the most important demands for successful imprinting is the presence of functional monomers in the polymer matrix. Their role is to assist in the creation of the specific binding sites in the cavity in an optimal position for rebinding. The wide choice of the functional monomers is a richness for the imprinting approach. However, most of the sol–gel MIP proposed in the literature do not fulfil the selectivity requirement for sensors and research is going on to overcome these limitations and to achieve a good selectivity towards the targeted analytes. Compared to organic MIP, sol–gel MIP materials display a high thermal stability, a versatile porosity and high specific adsorption surface. The ease of their preparation and the possibility to obtain optically transparent matrices are big advantages over organic MIP.

4. Innovative chemical sensors

4.1 Hybrid matrices with tailored pores

Undoped sol–gel matrices are mostly used as molecular sieves for the specific trapping of molecules by their size, but not as a sensing matrix. An example of the latter use is given here for the detection of volatile aromatic hydrocarbons. Hybrid xerogel matrices with tailored pore distribution have been synthesized for the reversible trapping of monocyclic aromatic hydrocarbons such as benzene and its mono- di- and trimethylated derivatives. When coupled with a specific millifluidic system and a detection *via* absorbance measurements, they allow the detection of these pollutants over the 100 ppb to 100 ppm range. Tran-Thi's group.[32] demonstrated that a pre-concentration step is not necessary and that the detection of aromatic hydrocarbons can be achieved in a single step.

Transparent monolithic disks (Fig. 4) were synthesized by these authors using two silicon alkoxide precursors, tetramethoxysilane (TMOS) and 3-aminopropyltriethylsilane (APTES), in the molar ratio 1 : 0.03. The mesoporous matrix displays large pores with a narrow distribution (36 ± 20 Å) which allow the rapid diffusion of the aromatic molecules into the porous network.

With a single monolithic and transparent xerogel disk whose diameter and thickness are 3 and 0.5 mm respectively (Fig. 4), Crunaire and Tran-Thi[33] have shown that these volatile organic pollutants can be trapped in the disk exposed to a small gas flow (100 mL min^{-1}).

The absorption spectra are collected as a function of time with a miniature spectrometer from Ocean Optics. The pollutants can be directly detected and identified *via* their spectral fingerprints over the UV domain (Fig. 5) by deconvolution of the collected spectrum. With a new type of millifluidic cell, the trapping is efficient and is reversible *via* purging the monolith with neat air at a high flux (3 L min^{-1}) after each exposure. The exposure time lasts 30 s and the whole cycle of trapping-detrapping 5 min (Fig. 5).

The limit of detection is 100 ppb for benzene with a 30 s sampling time over the whole range of relative humidity from 0 to 94%. This sensor is devoted to the control of the exposure of workers in petrochemical industries. The interference with potential solvents encountered in petrochemical industries such as acetone, which displays an absorbance in the UV domain of interest, was checked and found to be negligible due to their very low absorption coefficient in comparison with the corresponding aromatic compounds.

The use of undoped matrices for sensors is very scarce compared to the wide domain of hybrid matrices doped with reactants. In the next section, we will focus on the most selective chemical sensors which make use of specific chemical reactions to obtain the desired selectivity.

4.2 Doped matrices with tailored pores

The majority of the doped matrices reported in the literature involve the entrapment of fluorescent or phosphorescent dyes

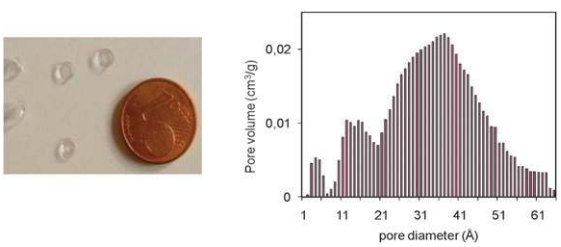

Fig. 4 Left: Mesoporous monolithic and transparent disks for the reversible trapping of aromatic monocyclic hydrocarbons. Right: Distribution of micro- and mesopores obtained from the analysis of the BET adsorption-desorption isotherms using the differential functional theory model.

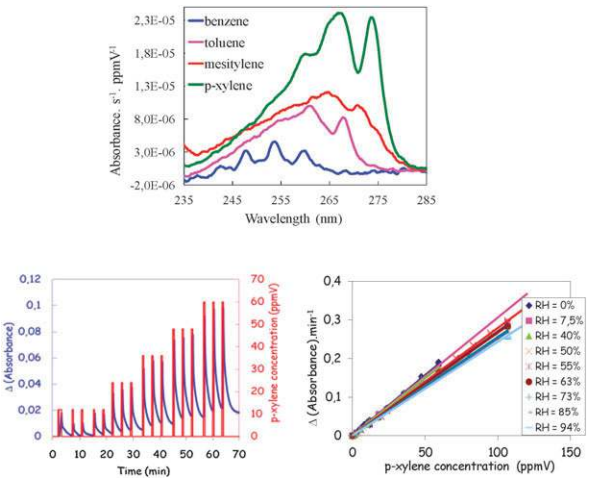

Fig. 5 Top: Normalized spectra of each compound trapped in the matrix expressed in absorbance per unit of the disk thickness, per unit time of exposure (seconds) and per unit concentration (ppmV). Bottom left: Kinetics of p-xylene trapping and detrapping followed by the absorbance measurement at 276 nm. Bottom right: Calibration curves for p-xylene trapping over a wide range of gas humidity (0–95%).

for the detection of small ions (proton or metallic ions) and small molecules such as O_2, CO_2, NO_2 and NH_3. Though most of these sensors were cited or thoroughly described in various reviews[1,2] we have chosen to detail a few innovative sensors of CO_2 and O_2, which make use of low cost technologies.

In the first work, the authors report a CO_2 sensor which employs fluorescence energy transfer and lifetime measurements as optical transduction method.[7] Their approach combines the use of a colourimetric pH indicator such as the Sudan III dye and the inert long-lived fluorescent ruthenium(II)-tris(4,7-diphenyl-1,10-phenanthroline) complex co-immobilized in the same hybrid ormosil–ethyl cellulose film. To provide the necessary amount of water needed for the dissolution of CO_2 in the film, a hydrated quaternary ammonium, tetraoctylammonium hydroxide base was added, its function is also to stabilize the deprotonated form of Sudan III dye. When CO_2 is dissolved in the film, HCO_3^- is stabilized *via* ion pairing with the tetraoctyl ammonium ion and the Sudan dye is protonated.

The emission band of the Ru complex overlaping the absorption band of the pH indicator (Fig. 6), the fluorescence of the Ru complex is dependent of the CO_2 concentration. Its lifetime, τ, measured with the low-cost technique of phase fluorimetry is converted to phase data, θ ($\tan\theta = \omega\tau$, w being the angular modulation frequency). The phase angle variation between the non-exposed and the exposed film is obtained (see Fig. 7).

The sensor displays 11.2° phase shift between the limit of detection (0.06%) and 100% CO_2 with a resolution of 2% and responds linearly over this domain of CO_2 concentrations. The sensor is however sensitive to the humidity and calibration curves for different humidity levels must be achieved. The time response of the sensor is very short, in the order of 20 to 30 s.

Sensor array strategy is in the heart of low-cost sensors. The following example witnesses this trend with optical sensors with integrated light sources. Bright's group, by using pin printing technology in concert with sol–gel processing, had produced O_2 microsensor units that are spots of 100 μm of diameter and 1 μm thick, directly deposited on the face of a light emitting diode.[34] The LED serves as excitation source to excite the luminescent chromophores sequestred in the sol–gel material and the luminescence is detected with a CCD camera.

The fabrication of the pin printed optical sensor and integrated light source (PPOSAILS) proceeds in three steps (Fig. 8). In the first step, the LED dome-like portion is removed to form a planar surface. In step 2, a thin layer (~1 μm) of xerogel is deposited by spin-coating on the plane surface to smooth it. As the LED sources display a piedestal in the red domain of wavelength which could interfere with the luminescence signal, in step 2′, a thin layer of a red-tail absorber is deposited *via* spraying the paint solution (~120 μm). In the final step 3, the authors use a ProSys 5510 system (Cartesian Technologies) with model CMP-3 pins (Telechem) to print the luminophore-doped sol–gel solution onto the sol–gel base film (step 3) or paint layer (step 3′).

With the tris(4,7′-diphenyl-1,10′-phenanthroline) ruthenium(II) chloride pentahydrate sequestred in a hybrid n-propylTMOS/TMOS xerogel for the detection of O_2, the authors could observe with the CCD camera changes in the intensity of the colour upon excitation with the LED.

It can be observed that the response of the units drastically depends on their position on the surface of the LED, the light being more intense in the central part (Fig. 9). This problem can be resolved with a calibration of the intensity. However, the biggest challenge remains the choice of the paint layer, whose function is to filter the red pedestal of the LED light but whose absorbance could hinder the luminescence of the luminophore, leading to an irreproducible calibration curve. If this problem could be resolved, the PPOSAILS should provide a simple technology well suited for low cost sensors.

Usually, intensity-based detection in the absence of a reference could suffer from drift and instability due to instrumentation fluctuation (light source or detector drifts) and/or degradation or leaching of the sensitive probe. These limitations were overcome by combining sensor arrays with artificial neural network model.[35] Briefly, sensor arrays were produced *via* pin-printing deposition technique. They consisted of cubic arrays of O_2 sensing dots (diameter 210 μm, thickness 1.5 μm) deposited onto microscope slides (Fig. 10). Each sensing element comprised two ruthenium complexes, (tris(2,2′-bipyridyl) ruthenium(II) ($[Ru(bpy)_3]^{2+}$) and tris(4,7-diphenyl-1,10-phenanthroline) ruthenium(II) ($[Ru(dpp)_3]^{2+}$), encapsulated within a hybrid matrix composed of TEOS and n-octyltriethoxysilane. The two ruthenium complexes which are structurally similar possess similar absorbance and emission spectra but exhibit very different lifetime τ_0 values. Such characteristics are advantageous since it requires the same light source, optical filter and detector while their sensitivity towards O_2 quenching is different. The modulation of the response was then achieved by varying the different ratios of the two ruthenium complexes in each dot of a row.

Detection was performed in a home-built flow cell involving a laser (442 nm), an epi-fluorescence microscope, and a charge coupled device (CCD) detector. The authors observed that the

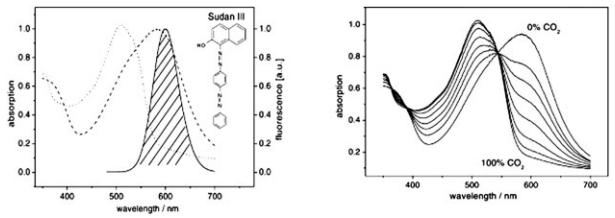

Fig. 6 Left: Absorption spectra of Sudan III: neutral (dashed line) and protonated (dotted line) and fluorescence spectrum of Ru complex (solid line). Right: Spectral evolution of Sudan III immobilized in ethyl cellulose when exposed to 0, 1.5, 3, 6, 12, 25, 50 and 100% of CO_2. Relative humidity of the gas mixture (N_2 + CO_2): 90%. From ref. 7.

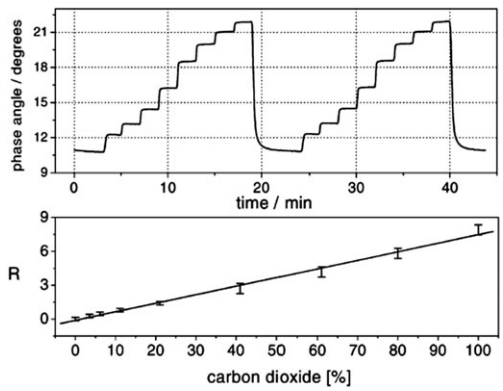

Fig. 7 Detection of CO_2 in gas mixtures *via* fluorescence phase modulation. Top: phase response of the sensor to 0,1.5, 3, 6, 12, 25, 50 and 100% of CO_2 at 90% of relative humidity. Bottom: Calibration plot obtained with $R = kpCO_2 = (\cot\theta_0 - \cot\theta)/(\cot\theta - \cot\theta_{max})$ where the subscripts 0 and max correspond to conditions where Sudan III is in its neutral and totally protonated forms, respectively. From ref. 7.

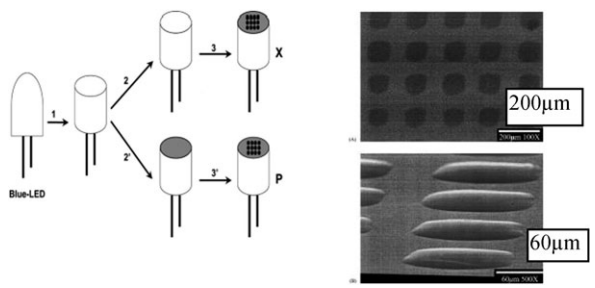

Fig. 8 Left: Production of PPOSAILS without absorber (1-2-3) or with (1-2′-3′) a LED red tail absorbing layer. Right: SEM images of the face of a PPOSAIL. Top view normal to the LED surface. Bottom: side view at 45° to the normal surface. From ref. 34.

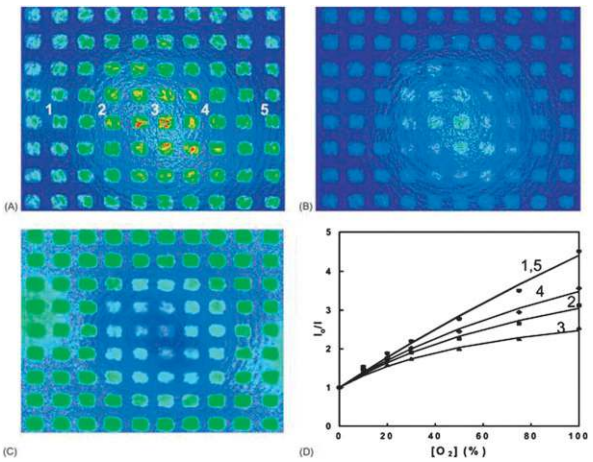

Fig. 9 Response of the PPOSAILS doped with the Ru complex and exposed to gas mixtures containing O_2 at various concentrations. False colour images A: under pure N_2, B: with O_2, C: recovered I_{N_2}/I_{O_2}. D: Stern–Volmer plots for the sensor units numbered 1 to 5 in panel A.

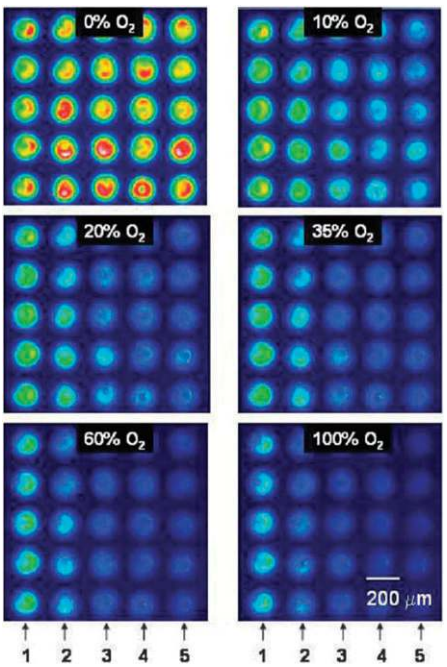

Fig. 10 O_2-dependent false colour images from an array of O_2 responsive xerogel-based sensor elements. Composition (mol%): x $[Ru(bpy)_3]^{2+}/(1 - x)$ $[Ru(dpp)_3]^{2+}$. Sample 1: $x = 1$, Sample 2: $x = 0.75$, Sample 3: $x = 0.50$, Sample 4: $x = 0.25$, Sample 5: $x = 0$.

sensitivity decreased with decreasing amount of $[Ru(dpp)_3]^{2+}$. It was attributed to the difference in the τ_0 values of the two ruthenium complexes and their respective fraction within each sensing dot. Artificial neural network (ANN) algorithms were used to analyse and identify the CDD images from the array. The authors demonstrated that the combination of such sensor array with the ANN algorithm yielded to a 5–10 fold improvement in accuracy and precision compared to a single-element sensor for quantifying O_2 in unknown samples. This approach (sensor arrays combined to the ANN algorithm) was also tested for detection of O_2 in rat plasma/blood. Despite a significant decrease in the sensor response due to blocking effect of rat plasma/blood components towards O_2 diffusion, the response of sensor arrays remained stable after 15 minutes.

Another way avoiding limitations of luminescence intensity-based detection was provided by a modified DLR method which allowed sensing of pH and dissolved oxygen simultaneously.[6] Basically, the DLR method is based on the combination of two fluorophores: an analyte-insensitive long-life time fluorophore (with a decay time in the

microsecond range) and an analyte-sensitive fluorophore (with a decay time in the nanosecond range). DLR method requires the overlapping of absorption and emission spectra of both indicators. It allows then simultaneous excitation and detection of both luminophores with a single light source. During DLR experiments, the luminescence intensity of both dyes is converted into a phase shift which is related to analyte concentration. In contrast to the conventional DLR method, the modified method involves an analyte-sensitive long-life time fluorophore and then measurements of phase shift at two different frequencies allowing then the detection of two analytes, there pH and dissolved oxygen.

The two fluorophores used in this study were a pH-sensitive carboxyfluorescein dye and a O_2-sensitive ruthenium complex $[Ru(dpp)_3]^{2+}$. These two fluorophores were selected since they fulfil DLR requirements and they are compatible with low-cost LED and photodiode technology.

The pH-sensitive dye was covalently incorporated in polymer microbeads while the ruthenium complex was encapsulated into ormosil microparticles, both matrices providing a selective permeability for targeted analytes (protons or O_2). Doped polymer microbeads and ormosil microparticles (1–3 μm) were further dispersed into a polyurethane hydrogel membrane supported on solid transparent support (polyester support—Mylar®). This supported dually sensing membrane (10 μm) was glued to the tip of an optical fibre connected to the optical setup (Fig. 11).

Since the long-life time fluorophore ($[Ru(dpp)_3]^{2+}$) acts both as reference and as sensitive compound, a low sensitivity could result in a low precision in O_2 concentration and also in the calculated pH value. On the other side, if sensitivity to O_2 was too high, the overall phase shifts in dual sensor will be too low at oxygen saturation, resulting in low precision of pH sensing. There exists then a compromise in the sensitivity of the long-life time fluorophore which was provided by the ormosil matrix. Phase shifts were determined at two different frequencies (30 and 60 kHz) for different pH and oxygen concentration. Oxygen concentration and pH were calculated *via* mathematical equations with a good accuracy (error for $pO_2 < 15\%$ and for pH determination < 0.23 units). The error for O_2 concentration was attributed to difference in the temperatures between calibration (20 °C) and validating experiments (23 °C). Interestingly, this dual approach was successfully used to simultaneously measure the pH and dissolved oxygen during the growth of *Pseudomonas putida* bacterial cultures.[36]

In contrast to the tremendous number of works on the sensors of O_2, CO_2, NO_2 and NH_3, very few works reported the detection of volatile organic compounds over the ppb range. Tran-Thi's group.[37] have shown that formaldehyde, a ubiquiteous and carcinogenic indoor air pollutant can be selectively detected and measured using Fluoral-P, a probe molecule entrapped in a TMOS xerogel displaying micropores.

The "one pot" synthesis with TMOS/EtOH/H_2O in a 1/4/4 molar proportion and Fluoral-P 0.5 mol L^{-1}, allows a heavy doping of the xerogel, once dried (4 mol L^{-1}).[38] In the xerogel pores (diameter <20 Å), the reactivity of Fluoral-P molecules with formaldehyde is enhanced as compared with the liquid phase, due to the confinement of the reactants in the same pore. The product issued from the reaction, 3,5-diacetyl-1,4-dihydrolutidine (DDL), can be detected either *via* absorbance or fluorescence measurements (Fig. 12).

Xerogel thin films (200 nm) doped with Fluoral-P were obtained by dip-coating quartz or glass substrates in the sol. The dried films are then exposed to calibrated mixtures of formaldehyde using a home-made prototype (Fig. 13).

The response of the sensor exposed to a flux of gas mixture containing different concentrations of formaldehyde is shown in Fig. 14. It was found that the variation of DDL fluorescence with the exposure time varies linearly with the concentration of formaldehyde.

The response time of the sensor varies from 2 to 15 min over the concentration range of 1 to 200 ppb and over a humidity range of 0 to 85% and the detection limit is 400 ppt. Other aldehydes such as acetaldehyde, propanal, butanal, pentanal, hexanal and benzaldehyde do not interfere in the detection of formaldehyde.

In this work, the authors have shown that the strategy of using a TMOS xerogel which provides micropores suited for the trapping of formaldehyde and which allows a heavy doping of the pores with the probe molecules, was successful.

Another strategy focus on the microfluidic devices which can display above the miniaturisation many advantages such a reduced sample volume and an increased reaction speed (Fig. 15). The example here given combines this strategy with a judicious choice of the sensitive sol–gel layer to detect biphenyl at micromolar concentrations in aqueous solution.[39]

Lanthanide ions such as Tb^{3+} are known to weakly fluoresce in the visible with a green light when excited in the UV (273 nm). In solution, it is well-known that the interaction of excited states of polyaromatic hydrocarbons with the lanthanide ion results in an efficient energy transfer from the former to the latter inducing an enhancement of the lanthanide ion fluorescence. By immobilizing the cyclodextrin molecules in the xerogel matrix and trapping in the same cyclodextrin bucket Tb^{3+} and biphenyl molecules, the authors obtained an efficient chemosensor of biphenyl. Although the purging cycle is slow (1 hour), the time response of the sensor, corresponding to the fluorescence rise, is 10 min.

4.3 Doped matrices with nanostructured pores

POMMs were widely used for the detection of analytes in the liquid phase (mainly toxic metal ions and also, H^+, anions, amines) and in a lesser extent for the detection of gas or volatile compounds (O_2, methanol, TNT, BF_3, SO_2). A general trend was observed with POMMs-based sensors. They display an increase of sensitivity and a decrease of detection time compared to non-porous materials synthesised without surfactants. This can be explained by (i) an improvement of analytes diffusion inside matrices, (ii) a high loading of sensing molecules which are usually non-aggregated, and (iii) a high availability of sensing probes towards pollutant species since all the porosity is opened.

Three types of detection techniques have been used in these studies: visual colorimetric, UV-visible absorption-based and direct luminescence intensity measurements. The aim of this part is not to provide an exhaustive review on sensing

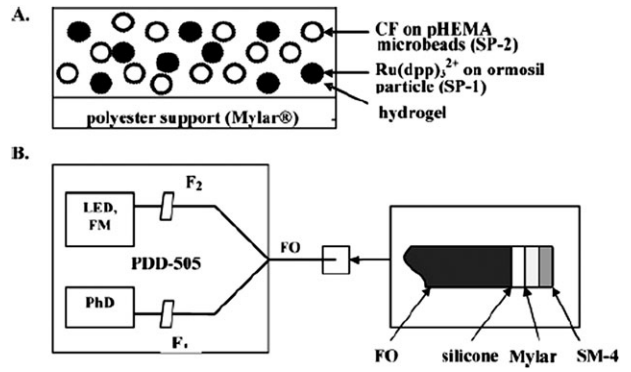

Fig. 11 (A) A schematic of the sensor membrane used for simultaneous optical sensing of oxygen and pH. The chemically sensitive materials are deposited on an inert mechanical support made from poly(ethylene glycol) (Mylar) that facilitates handling of the sensing films. (B) The optical setup and components used. LED, light-emitting diode; FM, frequency modulator; PhD, photodiode; F1 and F2, optical filters; FO, fiber optic cable; SM, sensor membrane that is glued to the tip of the fiber optic with silicone grease. The luminescence of the beads in membrane SM is excited through the fiber, and a fraction of their total emission is guided back through the fibers to a photodiode detector where phase shifts are determined.

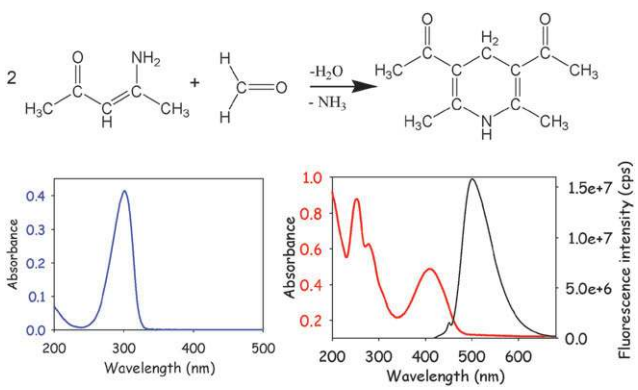

Fig. 12 The reaction of two molecules of Fluoral-P with formaldehyde producing DDL. Bottom left: Fluoral-P absorption band. Bottom right: DDL absorption (red) and fluorescence (black) spectra.

properties of POMMs (for a review on this field, see for example ref. 40). We will discuss on selected optical chemical sensors displaying interesting features such as low cost sensors, integrated devices, and versatile optical chemical sensors. These selected sensors illustrate also the different ways of POMMs functionalisation and involve the three types of detection.

Several parameters could greatly influence the diffusion rate of analytes inside POMMs such as textural (pore sizes, pore interconnection, pore morphology…) and structural characteristics of the mesophase, their surface charges (mainly depending of the chemical nature of oxide and or grafted species which could be neutral or positively or negatively charged) and their hydrophilic/hydrophobic balance. For example, it was demonstrated that three-dimensional mesophase (typically the *Pm3n* phase obtained with CTAB surfactant) allowed better analytes diffusion compared to a two-dimensional or a wormlike phase and even

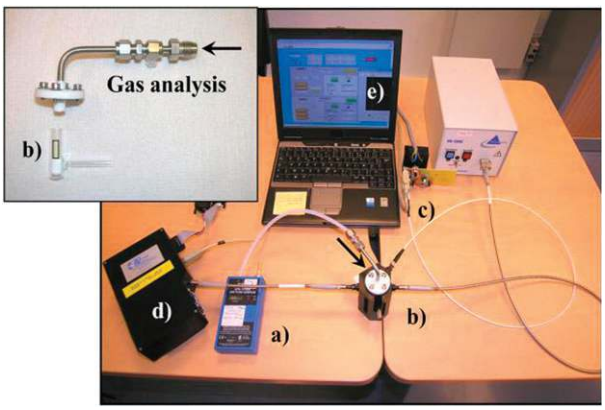

Fig. 13 Detection system. The atmosphere to be analysed is pumped *via* micropump (a) (220 mL min^{-1}) into a flow cell (b) containing the xerogel film. The flow-cell is inserted in a cell-holder (b) with optical windows is connected to a LED (or lamp) (c) and a miniature spectrophotometer (d) which measure the absorbance and fluorescence signal. The whole system and signal processing are driven with a computer (e).

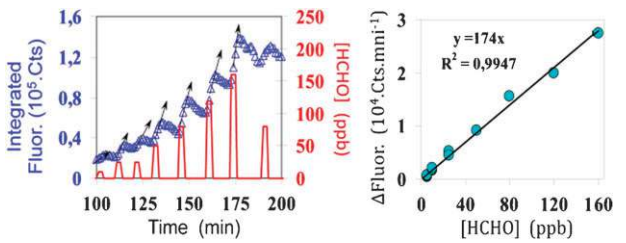

Fig. 14 Left: Fluorescence signals collected during the exposure of a xerogel thin film doped with Fluoral-P to gas mixtures containing various formaldehyde concentrations. The slope of the fluorescence intensity rise (left Y-scale) as function of time is proportional to the formaldehyde content in the gas mixtures (right Y-scale). Right: Calibration curve corresponding to slope values as function of CH_2O concentration.

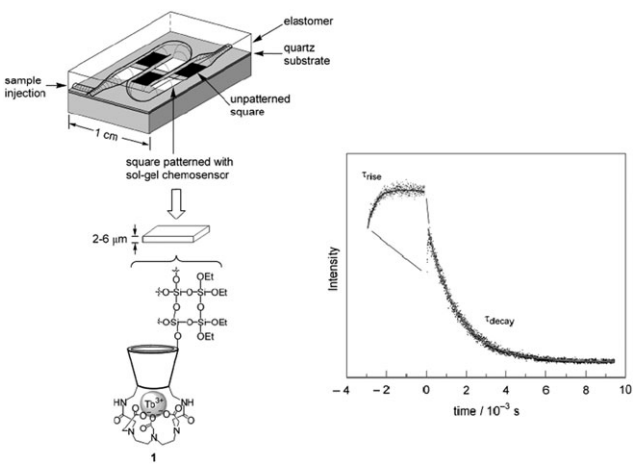

Fig. 15 A microfluidic chemosensor fabricated in a serpentine channel configuration. The sensor layer deposited on the treated surface (white squares) of the quartz slide, is composed of a TEOS xerogel to which are attached modified cyclodextrin molecules entrapping Tb^{3+} ions. Right: The fluorescence rise of TB^{3+} biphenyl fluorescence and decay of the signal by washing the sensor with methanol.

a 3D hexagonal mesophase (space group $P63/mmc$).[25] This tendency is amplified by the size of analytes. In the liquid phase, the diffusion of ionic species could also be favoured or hindered by the pH of solution. Since POMMs are in equilibrium with the liquid phase, their surface bears charges: positive if the pH is below the isoelectric point (IEP) and negative if the pH is above the IEP. At neutral pH, it implies then silica-based POMMs, which display an IEP about 2–3, could act as an electrostatic barrier for anions and as a preconcentration medium for cations, in addition to the sieving effects previously mentioned. The surface charge of POMMs could be easily adapted to the working sensing medium either *via* grafting of charged organosilanes or *via* the incorporation of transition metal oxides precursors presenting different IEP in the starting sol.

Visual detection of toxic metal ions *via* post-modified POMMs monoliths. In the past few years, El-Safty *et al.*[41,42] have developed toxic metal ion sensor strips based on naked-eye detection. Briefly, the authors synthesised POMMs shaped as disk-like membranes (thickness 0.05 cm/diameter 1.02 cm) by a casting method *via* the lyotropic liquid crystalline phase approach. Monoliths displayed either a cubic, 2D-hexagonal or wormlike mesostructure depending on the experimental conditions (surfactant, composition). After a calcination step at high temperature (500 °C) allowing the removal of template and stiffening of silica networks, an impregnation step with an ethanolic solution of hydrophobic non-commercial azo-probes (Fig. 16) was performed at room temperature under vacuum for 1–2 h. This post-modification led to an azo-probes loading around 10–15 wt% without damaging the mesostructure of monoliths. In a next impregnation procedure, the monoliths were washed with deionised water and dried at 60 °C for 45 minutes.

Sensing experiments consisted of simple immersion of sensors in solutions containing toxic metal ions at a given pH with or without interfering ions. Detection of toxic metal ions was done through complexation reaction between sensitive probes and metal ions which induced a bathochromic shift in the absorption spectra of probes (Fig. 17).

Interestingly, despite non-covalent bonds between matrices and sensitive probes, dye leaching was not observed over the whole sensing process (6 detection-regeneration-washing cycles). This probes retention was ascribed to both "short-range" interactions (*i.e.* van der Waals and hydrogen bond) between sensitive probes heteroatoms and silanol/silanolate moieties of silica surface and their high hydrophobicity provided by the added long alkyl chains.

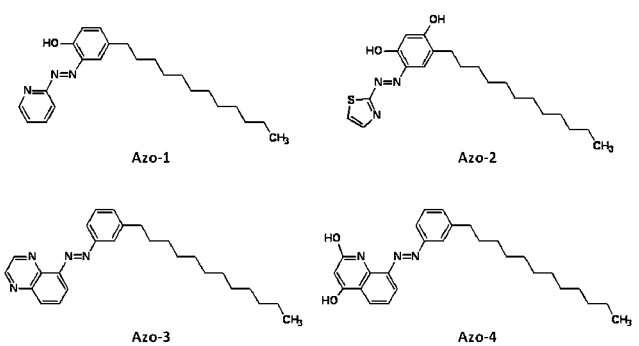

Fig. 16 The structure of chemically-synthesised azo chromophores with long hydrophobic tails.

In these studies, the effects of pH, temperature, pollutant sample volume, response time, and monoliths thickness were optimised for a fast visual detection of Hg(II) and Co(II) (similar studies involving the alternative route to the covalent grafting have been also reported by El-Safty *et al.*[41,42] for the naked-eye detection of Cr(VI), Pb(II), Pd(II), Sb(III), Bi(III), Cd(II)). The authors observed that an equilibrium time of 15 minutes at 25 °C was necessary to obtain a prominent colour and to reach signal saturation of strip reflectance spectra. It was also shown that this equilibrium time increased with the thickness of monoliths (up to 20 minutes for a 0.2 cm thick monolith) due to the analytes diffusion limitation. Moreover, thicker strips presented sensing difficulty in showing distinguishable colour changes during the detection of trace Hg(II)/Co(II) pollutants. They also observed that cubic monoliths in general presented a better sensing behaviour than wormlike monoliths, emphasizing then the importance of an ordered network for sensing applications.

In terms of sensitivity, these monolithic strips displayed a wide visual detection range between 1.0 and 200.0 ppb (depending on the system probes–metal ions) (Fig. 17). Sensor strips were simply regenerated by immersion in an aqueous solution containing a complexing agent (CH_3COO^- or EDTA for example) followed by a washing step with deionised water. No leaching of sensitive probes was observed during this regeneration step. However, a slight decrease of monoliths sensitivity was noticed after several detection/regeneration cycles. Reproducibility, which is also a key parameter in the sensors field, was tested over 10 analyses by UV-visible reflectance spectroscopy. The standard deviation was between 0.6 and 2.5%.

An important issue related to sensor workability is the selectivity factor. In this sense, several experiments were conducted. Interfering species were first identified *via* experiments in solution involving the azo-probes and transition, alkali metal and alkaline earth metal ions. Next, the same experiments were done with sensitive monolithic strips. It was

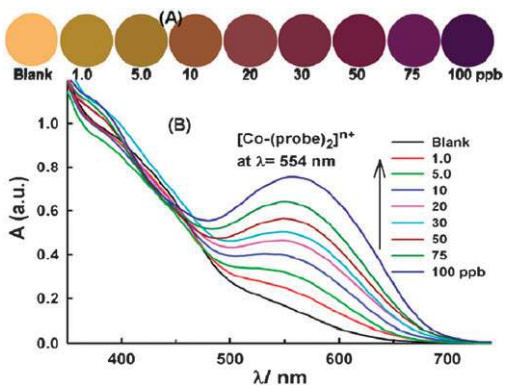

Fig. 17 Colour transition map (A) and reflectance spectra (B) observed for 2D-hexagonal monolithic strips doped with the Azo-4 probe in optimised experimental conditions: pH of Co(II) solution = 5.5, total volume 20 mL, equilibrium time 15 minutes, temperature 25 °C, disk membrane thickness 0.05 cm.

observed that monolithic strips did not display colour changes even if the concentrations of interfering species were higher than those of analytes (Hg(II) or Co(II)). Interference studies were extended by adding Hg(II) or Co(II) analytes after the addition of interfering species. In these interfering systems, the azo-probe modified sensor exhibited a good tolerance for interfering species (tolerance concentrations of these species were 50–100 times higher than those of analytes). Finally, simulated wastewater or real sample effluents were used for testing monolithic strips. The recognition of Hg(II) or Co(II) was visualised by naked eye detection and quantitatively determined by UV spectra with a good accuracy. In term of stability, it was demonstrated that these monolithic membranes presented a "shelf time" of several months.

Direct luminescence intensity detection of pH with functionalised POMTFs-based microfluidic/photopatterned devices. In 2000, Brinker's group elaborated a patterned pH-sensitive fluidic system. Patterns of hydrophobic surface assembled monolayers (SAMs) were printed with a polydimethylsiloxane (PDMS) stamp and an ink containing a long alkyl chain organosilane (octadecyltrichlorosilane) (Fig. 18).[20] The sensor device consisted in L-shaped patterns with a viewing cell, created by interdigitating long narrow lines with large pads on the ends used to load solutions. After an appropriate treatment, the patterned substrat was immersed in a solution containing TEOS, Brij-56, H_2O, ethanol, HCl and the coupling agent, 3-aminopropyltrimethoxysilane. Evaporation of ethanol during dip-coating increases the hydrophilicity of thin film leading then to its selective de-wetting on the hydrophobic surface of SAMs. A calcination step at moderate temperature allowed the removal of surfactant while maintaining the amine functionality. The functionalisation of POMTFs was achieved by the combined approach developed in the previous chapter. The dye conjugation reaction was realised by immersion of patterned amine-functionalised cubic POMTFs in a solution of 5,6-carboxyfluorescein succinimidyl ester (5,6-FAM SE).

Finally, solutions at different pH were placed on the pads and transported to the cell by capillary flow. The comparison of the fluorescence spectra indicated that dye molecules covalently attached to the mesoporous framework retain similar features to those in solution.

Wirnsberger *et al.*[12] produced a similar pH sensor involving a coupling procedure in the starting sol. Functionalised POMTFs were synthesised following the "one-pot" route by reacting fluorescein isothiocyanate with 3-aminopropyltriethoxysilane and adding it to a F127 block copolymer film solution. These sensors operated by recording the emission of the anchored fluorescein dye. Thin film sensors acted analogously to the dye in solution, except that the p*K*a value was shifted from 6.4 in solution to ~7.3 in thin films. The response time of the mesoporous hybrid thin films was about 7 s for a 95% change in the emission intensity. This response time is much shorter than the value measured in conventional sol–gel glasses. The fast response time was attributed to the high porosity of the dye-carrying mesoporous thin film, since the open pores enable a fast diffusion of the solution toward the dye molecules.

The same functionalisation approach was used to fabricate photopatterned pH sensors.[43] These sensors integrated selective ion-channel transport polypeptides (gramicidin A) embedded in a supported phospholipid bilayer with pH-responsive mesostructured and mesoporous silica-based arrays (Fig. 19). Briefly, after dip-coating a mesostructured thin film functionalised with fluorescein derivatives on silicon wafer

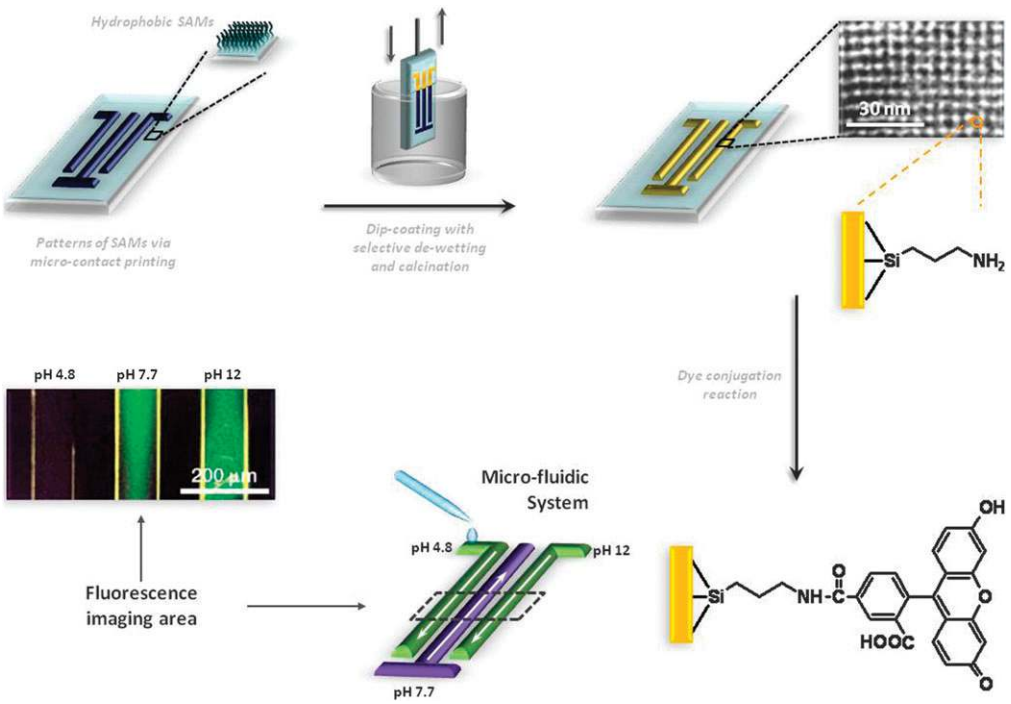

Fig. 18 Patterned pH-sensitive POMTFs formed by a selective de-wetting. Copyright © 1999 Nature Publishing Group.

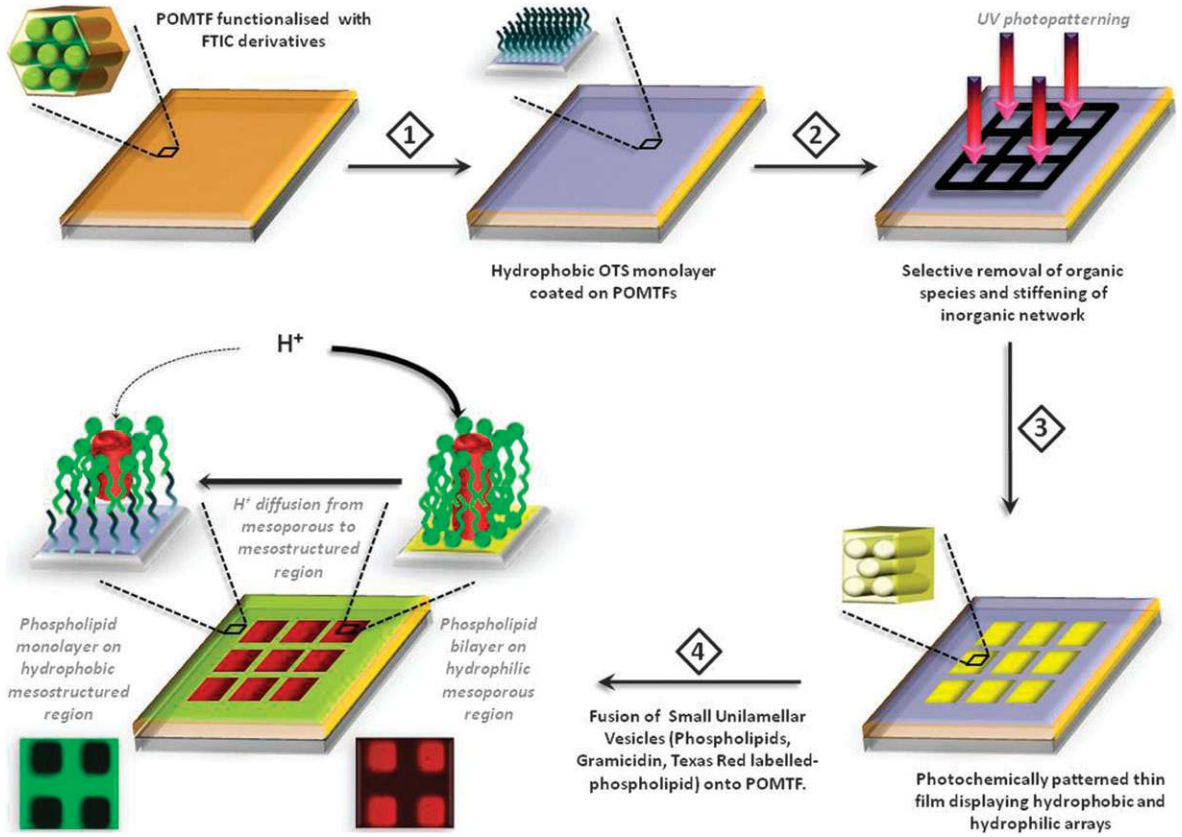

Fig. 19 A scheme representing the main steps in the design of multifunctional sensing platform.

substrate, thin films were coated with a hydrophobic monolayer of n-octadecyltrichlorosilane (OTS). Next square-shaped patterns were produced by photolithography technique. Short-wavelength irradiation (184–257 nm) allowed both the removal of organic species (surfactant, OTS, fluorescein, aminopropyl) and the stiffening of the silica network. Surface of thin film was then composed of two distinct regions: (i) a hydrophobic surface composed of the OTS monolayer upon a pH-sensitive mesostructured thin layer and (ii) a square-shaped hydrophilic surface constituted by a mesoporous silica thin layer. Finally the patterned film was incubated with small unilamellar vesicles consisting of phospholipids and gramicidin. It resulted in the formation of a phospholipid bilayer on hydrophilic region and phospholipid monolayer on the hydrophobic OTS region. It was observed that phospholipid monolayer coated on the hydrophobic region was hardly permeable to H^+ due to the blocking effect of OTS monolayer on transmembrane proton transport. In contrast, the hydrophilic part enables the dimerisation of gramicin permitting thus a great improvement of proton transport towards POMTFs. These results also demonstrated the facile diffusion of analytes from mesoporous (POMMs after surfactant removal) to sensitive mesostructured regions (POMMs containing surfactant). The stability of phospholipid layers in aqueous medium over a wide range of pH coupled to the selectivity of ion-channel transport polypeptides coated on photopatterned sensitive POMTFs are a promising way towards detection of a broad range of species (ions and molecules).

Versatile optical chemical sensors. POMTFs functionalized with triethoxysilyldibenzoymethane (SDBM) exhibiting a high selectivity and sensitivity towards both metal cation pollutants such as uranyl and BF_3 gas were recently developed.[10,44] In these studies detection of metal cation pollutants was done by UV-visible absorption spectroscopy while detection of BF_3 was realised either by UV-visible absorbance or fluorescence intensity measurements.

Incorporation of the hydrophobic non-commercial silylated β-diketone SDBM species in POMTFs was achieved following the ''delayed procedure'' (addition of organosilanes just prior the sol deposition). Since the solubility of this organosilane in ethanol was extremely low, a part of ethanol was replaced by tetrahydrofuran (which solubilises SDBM more efficiently than ethanol without altering the formation of the mesostructure). The addition of increasing amounts of SDBM for a fixed CTAB/silica molar ratio (which usually leads to a cubic mesophase at high relative humidity without guest molecules) induced mesostructural evolutions in thin films. The following sequence was observed: cubic phase ($Pm3n$) < mixture of cubic ($Pm3n$) and 2D-hexagonal ($p6m$) < pure 2D-hexagonal phase < lamellar phase. Such phase transitions were explained by the preferential solubilisation of bulky hydrophobic SDBM species in the hydrophobic part of micelles during evaporation of solvents.

After a moderate thermal treatment and surfactant extraction in ethanol, the spectral responses of functionalised thin films with [SDBM]/[Si] molar ratios of 2.7 and 5.3% (2D-hexagonal $p6m$ and lamellar phases respectively) were

studied in aqueous solutions with various metallic cation salts: Cd(II), Ce(III), Co(II), Cr(III), Eu(III), Ni(II), U(VI), Cu(II) and Fe(III). Detection tests consisted in a simple immersion (30 seconds under gentle stirring) of thin films in an aqueous solution of metallic cations. The *in situ* monitoring during these first 30 seconds shown that optical changes occurred for three cations only (Cu(II), Fe(III) and U(VI)) in the UV domain and the formation of colored complexes for the last two cations only (orange with Fe(III) and yellow for U(VI)). The selectivity of films towards Cu(II), Fe(III) and U(VI) cations was explained by a shorter complexation equilibrium time compared to other metallic cations. Complexation kinetics were observed to be dependent upon the concentration of U(VI), ranging from seconds at high concentrations (above 100 ppm) to minutes at low concentrations (below 100 ppm). The uranyl detection limit was attained for a 1 ppm solution. This detection limit is relatively low if we consider the simple absorbance variation sensing method used and the thickness of samples (800 nm). It is worth mentioning that classical amorphous sol–gel functionalised thin films synthesised without surfactant showed similar UV-visible spectra but did not show efficient detection of any tested metallic cations. Finally, the reversibility and reproducibility of film were tested using repeated detection regeneration cycles. A simple treatment in solution with acetylacetone permits regeneration of the films with good preservation of their sensing properties, even after several complexation–regeneration cycles. For a 2D-hexagonal phase reproducibility was about 3% and, more surprisingly, about 7% for the lamellar structure. The stability of such a hybrid lamellar phase *versus* washing–complexation–regeneration cycles could be explained by the presence of π-stacking interactions between SDBM compounds located on the opposite sides of the silica layers.

The same SDBM-functionalized POMTFs were successfully used as selective sensor for boron trifluoride, a gas commonly used in semiconductor industries.

Thin films with cubic and lamellar structures were exposed to BF_3 and BCl_3 gas mixtures. The authors demonstrated that only BF_3 can selectively produce with the silylated β-diketone the corresponding (dibenzoyl)methanato boron difluoride ($SDBMBF_2$), which absorbs in the UV-visible and fluoresces over the visible domain (400–700 nm). BCl_3 does not interfere in the reaction (Fig. 20).

In the *Pm*3*n* thin film, the observed $SDBMBF_2$ fluorescence correspond to that of the $SDBMBF_2$ monomers. In contrast, the π-stacking interactions between SDBM compounds in the lamellar thin films is witnessed by the dual fluorescence bands observed in the emission spectrum, the broad band at low energy being attributed to the fluorescence of $SDBMBF_2$ dimers. The sensor can be recycled by washing the thin film with alcohol to recover the initial SDBM probe molecules.

Cationic surfactants: template and sensitive probe. A large number of articles are devoted to mesostructured porous thin films obtained with cationic surfactant as templates as described in section 3. In all cases, the surfactant molecules are washed out of the pores to leave void spaces, which can later be used to entrap other compounds. Contrasting with this strategy, Tran-Thi's group.[45] made use of cationic surfactants (cetyltrimethylammonium bromide (CTAB) or decamethonium dibromide (DCMdiB)) as a probe molecules to detect traces of gaseous chlorine. Their strategy was to reproduce a well-known oxidation reaction of bromide ion, Br^-, by chlorine, Cl_2, which usually occurs in solution as follows:

$$2Br^-(aq) + Cl_2(aq) \rightarrow Br_2(aq) + 2\,Cl^-(aq) \quad (1)$$

$$Br^-(aq) + Br_2(aq) \Leftrightarrow Br_3^-(aq) \quad (2)$$

In the presence of an excess of Br^-, the tribromide ion, Br_3^-, is formed, which absorbs intensely at 270 nm.

These authors have shown not only that the reaction can take place in the porous sol–gel matrix, but also that it is much faster in the nanoreactor than in the liquid phase. This is due to the proximity of the Br^- ions present in the same pore, in particular when the CTAB micelles are formed displaying a dense crown of the Br^- counter-ion.

In these nanostructured thin films, the diffusion of a small molecules such as Cl_2 is very fast. A 30 s exposure of a thin film doped either with cetyltrimethylammonium bromide or with decamethonium bromide was sufficient to detect Br_3^- with traces of Cl_2 in the ppb range (20–850 ppb) (Fig. 21).

When CTAB micelles are formed in the pores, the authors showed that in the presence of an excess of Cl_2, a fast reaction between Br_3^- with Cl_2 occurs leading in few tens of seconds to the $BrCl_2^-$ species. This last reaction is also known to occur in solution *via* various reactions in equilibrium involving the Br_2Cl^-, BrCl and $BrCl_2$ species.[46]

4.4 Molecular imprinted sol–gel materials

Though the majority of molecular imprinted systems concern organic polymers, recent advances in molecular imprinted sol–gel materials have proved to have some advantages such as a thermal stability, which allows an easy removal of the organic templates *via* heating at high temperature. Walker *et al.*[3] used a hybrid strategy developed by Whitcombe *et al.*[31] involving polymerisable monomers possessing a covalently bound template molecule to detect explosive gas, trinitro toluene (TNT). Bis(trimethoxysilylethyl)benzene (BTEB), a silane containing a phenyl bridging group was used as a precursor for the silicate matrix (Fig. 22).

Following the co-polymerisation of the template with BTEB, the template was removed *via* the cleavage of a carbamate linkage yielding a shape-selective binding site displaying an amine group. The gaseous TNT bound in the pocket is deprotonated to form the corresponding anion which is stabilized by the electron-withdrawing NO_2 groups and the protonated ammonium counter ion. The TNT anion is detected *via* its strong absorbance in the visible (λ_{max} = 532 nm).

Integrated optical wave guide spectrometry was used as transduction mode. The technique involves a longitudinal total reflection of the probe beam through a TiO_2/SiO_2 waveguide layer which allows 10^3 to 10^4 reflections per cm (Fig. 23). The sensor displays a high sensitivity of 5 ppb for a sampling time of 60 s at a flow rate of 40 mL min^{-1}.

However, it can be noted that many pollutants present in the atmosphere such as aldehydes and in particular the

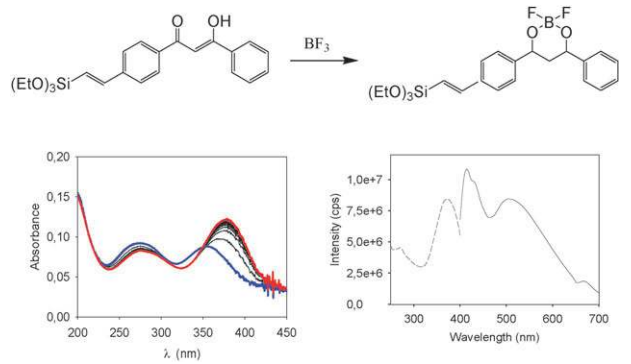

Fig. 20 Top: Reaction of the silylated β-diketone with BF_3. Bottom left: Spectral variations observed upon exposure of a lamellar thin film functionalized with SDBM (15 mol.%) (blue) to BF_3 (500 ppm) and progressive formation of $SDBMBF_2$ (red) issued from the reaction of SDBM with BF_3. Bottom right: (—) fluorescence spectrum collected upon excitation of $SDBMBF_2$ at 375 nm. (---) excitation spectrum collected with emission at 500 nm.

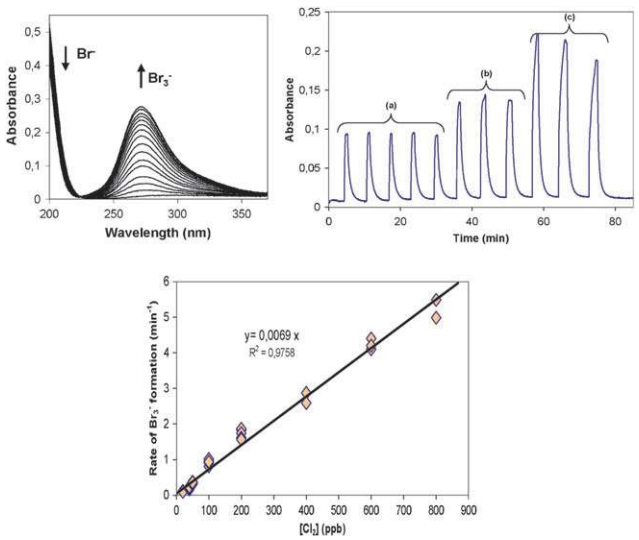

Fig. 21 Top left: Spectral variation of a film doped with DCMdiB upon continuous exposure to 190 ppb of Cl_2 during 1500 min, flux: 500 mL min^{-1}.Top right: Response of the chemical sensor exposed during 20 s to a flux of Cl_2 with various concentrations (a = 50, b = 100, c = 200 ppb) followed with a purge with clean air. Bottom: Calibration curve corresponding to the slope of the response signal as a function of the Cl_2 content in the gas mixture.

ubiquitous and reactive formaldehyde could also bind to the NH_2 functional groups and therefore the sensor could lack in selectivity.

The strategy of molecular imprinting can also be coupled with a fluorescence transduction strategy. The following work gives a good example of how photoinduced electron transfer (PET) between the targeted analyte and the functional group is used to produce a sensor of 2,4-dichlorophenoxyacetic acid, a toxic herbicide.[47] The authors use a functional monomer, the 3-[*N*,*N*-bis(9-anthrylmethyl)amino] propyltriethoxysilane (*N*,*N*-diAn) (Fig. 24), whose fluorescence is quenched due to the PET between the nitrogen doublet of the amino group to the anthryl (An) moieties. The fluorescence of the anthryl

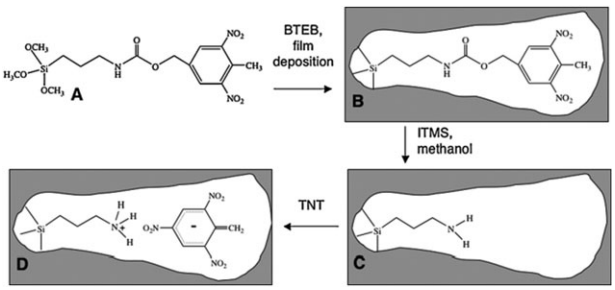

Fig. 22 Molecular imprinting scheme for the TNT sol–gel sensing layer. (A) The template (ex. **1b** shown). (B) Template is co-polymerized with BTEB by base-catalyzed hydrolysis and condensation of alkoxysilane groups. (C) The template is removed by cleaving the carbamate linkage using iodotrimethylsilane and methanol. (D) A shape-specific pocket aids in binding TNT. The amine group can TNT and deprotonate the methyl group to convert TNT into its anionic form (one resonance structure of TNT is shown).

moieties can however be recovered *via* protonation of the amino group in neutral pH or acidic media.

The authors make use of these properties to detect 2,4-dichlorophenoxyacetic acid (2,4-D) in a hybrid matrix with an intrinsic pH close to 7.7. The hybrid matrix was synthesized using as co-precursors tetraethoxy silane and phenyltrimethoxysilane and as functional monomer, the *N*,*N*-diAn and as template the 2,4-D analyte. After polymerisation, the 2,4-D was extracted. In the resulting MIP matrix, the *N*,*N*-diAn is weakly fluorescent.

When 2,4-D is trapped in the matrix, it interacts with *N*,*N*-diAn *via* acid-base interaction leading to the protonation of *N*,*N*-diAn and formation of 2′,4-D anion (Fig. 25). The consequence is an increase of the fluorescence intensity.

Here again, the selectivity remains a key point which is not solved since any organic acid with a similar size and shape, such as phenol derivatives would be able to interact with the *N*,*N*-diAn *via* an acid-base reaction.

With the following example, Bright's group proposed with the selectively templated and tagged xerogels (SSTTX) a new strategy to gain in selectivity.[48] The SSTTX protocol, which exploits a novel bifunctional sacrificial template (BST) in concert with sol–gel derived xerogel, is illustrated in Fig. 26.

The idea is to get two binding sites to bind the target analyte, 9-anthrol. A bifunctional sacrificial template is first synthesized (step a) and grafted to a TMOS xerogel in a one pot synthesis (step b). The chemical cleavage liberates two functional amino sites (step c), one of which is used to covalently attach a fluorophore, 4-chloronitrobenzo-2-oxa-1,3diazole (NBD-chloride), and the other to link 9-anthrol *via* a hydrogen bond (step d). An active SSTTX-based sensor is produced by removing the 9-anthrol.

The detection is based on the collection of the fluorescence signal of the NBD moiety, which is enhanced in the presence of 9-anthrol (Fig. 27 left). With this strategy, the authors can detect 0.3 μM of 9-anthrol with a time response of 45 s.

The reaction is totally reversible and the standard deviation is 6% after 25 cycles. The sensor exhibits a high selectivity of more than 290 for 9-anthrol over structurally similar

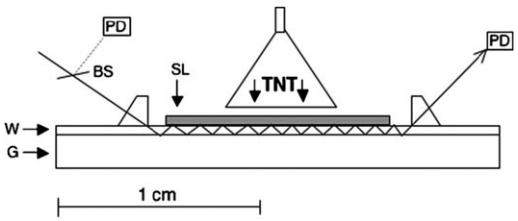

Fig. 23 A schematic of the TNT chemical sensor (note the vertical dimension is not to scale). G: glass support, microscope slide 1 mm in thickness. W: waveguide layer high index SiO_2/TiO_2 glass layer formed from sol–gel film deposition, thickness 0.8–1.0 μm. SL: molecularly imprinted sol–gel sensing thickness ~0.3–1.0 μm. BS: beamsplitter. PD: photodiode. A laser is prism coupled into the waveguide layer where the propagating beam interacts with the sensing layer upon each internal reflection. The intensity of the outcoupled light is measured.

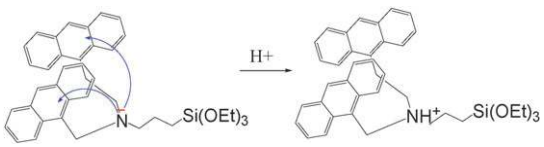

Fig. 24 The neutral 3-[*N*,*N*-diAn] is weakly fluorescent due to the intramolecular charge transfer from the nitrogen doublet to the macrocyclic ring. The fluorescence of the An moieties is recovered when the amino group is protonated.

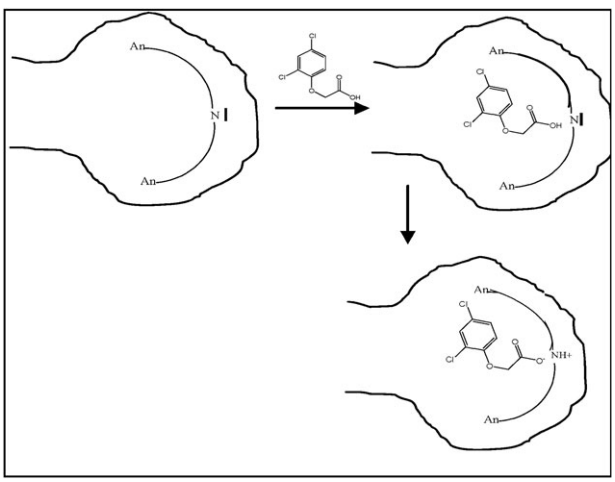

Fig. 25 Strategy of molecular imprinting combined with a PET dependent fluorescence. From ref. 47.

analogues such as anthracene, naphthol, phenol, 9,10-anthracenediol (Fig. 27 right).

All the optical sol–gel chemical sensors described in this section are collected in Table 1 for comparative purposes.

Conclusions

In this tutorial review, we attempt to give a general overview of optical chemical sensors based on hybrid sol–gel materials with a particular emphasis on both strategies of synthesis of efficient hybrid nanoreactors and production of advanced sensing platforms. We have shown that an extremely wide variety of nanoreactors can be achieved, from conventionally

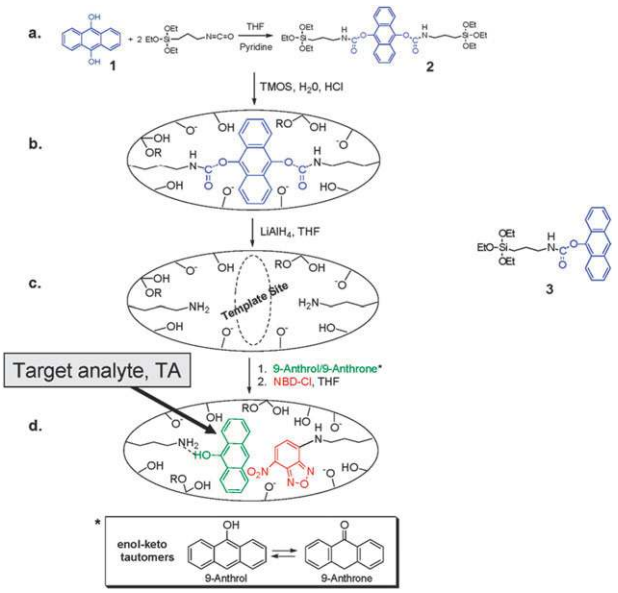

Fig. 26 Reaction protocol for producing an SSTTX for the selective detection of 9-anthrol. The sol–gel sensitive layer is 2 μm thick. From ref. 48.

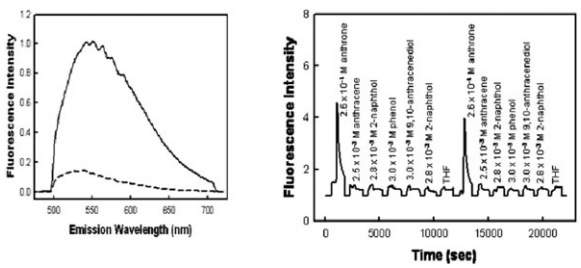

Fig. 27 Left: Steady-state emission spectra from a 9-anthrol-responsive, NBD-tagged SSTTX (s) and a control B xerogel (---) powder. λ_{ex} = 465 nm. Right: Fluorescence intensity *versus* time plot for a typical 9-anthrol-responsive SSTTX powder when it is challenged by a series of structurally similar analogues (potential interferences) with higher concentrations than that of the analyte. λ_{ex} = 465 nm. λ_{em} = 535 nm. Flow rate, 1.2 mL/min.

doped hybrid matrices to periodically organised mesoporous materials (POMMs) and molecular imprinting sol–gel polymers (MIP). With the examples given of nanoreactors, there seems to be no limit to the creative production of new sol–gel sensors. On the transduction side, the recent developments and improvements of sensing platforms (optical fibers, planar waveguides, cheap light sources, miniaturisation of detectors, micro- or millifluidic devices) are promising in terms of simplification and cost of the sensors for a targeted mass production. In the examples given, some of these two aspects were developed but, to the best of our knowledge, no sensors involving all of them have been reported. It is noteworthy that only a minor part of the sensors proposed in the literature had been industrialized such as O_2 (Presens GmbH), CO_2 and pH sensors (Gas Sensors Solutions). The main demands for a technology transfer being the selectivity of the sensor, the reproducibility of the synthesis process, the production of materials with reproducible properties and their storage

Table 1 Properties of the optical chemical sensors described in section 4

Analyte	Reactants	Materials	Detection	Sensitivity	ref.
Aromatic monocyclic hydrocarbons	None	TMOS + APTES monolith	Absorption and spectral deconvolution	100 ppb, 30 s	32
CO_2	Sudan III, tris(4,7-diphenyl-1,10 phenanthroline) Ru(II) chloride tetraoctylammonium hydroxyde	Ormosil–ethyl cellulose film	Fluorescence energy transfer and lifetime	0.06%, 20 s	7
O_2	Tris(4,7′-diphenyl-1,10′ phenanthroline, Ru(II) chloride pentahydrate	n-Propyl TMOS/TMOS xerogel	Fluorescence with PPOSAILS		34
O_2	Tris(2,2′-bipyridyl) Ru(II), tris(4,7-diphenyl-1,10-phenanthroline) Ru(II)	TEOS + n-octyl-triethoxysilane xerogel film	Sensor array and CDD images artificial neural network	O_2: 10% 15 min	35
O_2, pH	Tris(4,7-diphenyl-1,10-phenanthroline) Ru(II), carboxyfluorescein dye	Ormosil particles (SP-1) and pHEMA microbeads (SP-2)	DLR method, fluorescence lifetime	$pO_2 < 15\%$ 0; 23 pH unit	6
CH_2O	Fluoral-P	TMOS xerogel film	Fluorescence	400 ppt/15 min, 10 ppb/2 min	38
Biphenyl	Tb^{3+}, cyclodextrin	Xerogel	Luminescence	10 min	39
Metal ions	Azo-chromophores	Post-modified POMM monolith	Reflectance Naked eye	1 ppb/15 min	41 and 42
pH	5,6-Carboxy-fluorescein succinimidyl ester	Patterned functionalized cubic POMTF	Fluorescence imaging		20
pH	Fluorescein isocyanate	Functionalized POMTF	Fluorescence	7 s	12
pH, ion channel transport	Fluorescein	Phospholip monolayer on hydrophobic mesostructured OTS & phospholipid bilayers on hydrophylic mesoporous silica	Fluorescence		43
Metal cation, uranyl, BF_3	β-diketone	Functionalized POMTF	Absorption fluorescence	Uranyl: 1 ppm/30 s	10 and 44
Cl_2	Cetyltrimethylammonium bromide or decamethonium dibromide	POMM film	Absorption	20 ppb/30 s	45
TNT	Silylated DNT	Molecular imprint sol–gel layer, Bis(trimethoxysilylethyl) benzene	Wave guide and absorption	5 ppb/60 s	3
2,4-Dichloro phenoxyacetic acid	3-[*N*,*N*-bis(9-anthrylmethyl)amino) propylethoxysilane	Molecular imprint, TEOS/ Phenyltrimethoxysilane	Fluorescence	45 μM	47
9-Anthrol	4-Chloronitrobenzo-2-oxa-1,3diazole	Selectively template and tagged xerogel	Fluorescence	0.3 μM/45 s	48

lifetime, the sol–gel community still has to demonstrate these potentials. During the writing of this review, though we have found many examples of surface plasmon sensors (SPR) or surface enhanced Raman spectroscopy (SERS) using particularly attractive low-cost detection systems, none of them referred to hybrid sol–gel materials while biosensors represent the largest part.[49,50]

As was stressed previously by Borisov and Wolfbeis,[51] optical chemical sensor technology is not a matter of spectroscopy only, or of materials science, or of engineering or any other single discipline, but rather requires various scientific expertise in order to end up with a viable advanced sensor. One could then imagine advanced matrices combining the MIP approach of POMM materials and ''one-pot'' encapsulation of Au/Ag nanoparticles with SERS techniques. Such matrices could be easily integrated in microfluidic/photopatterned/optical fibres systems where the detection will be performed *via* miniaturised low cost optical setups (LED and photodiode).

Because of length restriction, we have omitted the domain of optical sol–gel biosensors which merits a review by itself. Since the first reports on the sol–gel encapsulation of enzymes in the early 1970s[52] and the real development of this process with the work of the Jerusalem group in 1990,[53] a tremendous number of works have appeared in the literature. The readers could get an idea of the development of this area through many reviews.[54–56] In particular, the discovery of new silicon precursors such as diglyceryl silane,[57–59] which allows the encapsulation of a large variety of biomolecules (liposomes, proteins, enzymes...) with improved storage stability, has led to a large number of optical biosensors.[60–62]

Notes and references

1 C. McDonagh, C. S. Burke and B. D. MacCraith, *Chem. Rev.*, 2008, **108**, 400–422.
2 O. S. Wolfbeis, *J. Mater. Chem.*, **15**, 2657–2669.
3 N. R. Walker, M. J. Linman, M. M. Timmers, S. L. Dean, C. M. Burkett, J. A. Lloyd, J. D. Keelor, B. M. Baughman and P. L. Edmiston, *Anal. Chim. Acta*, **593**(1), 82–91.
4 C. Huber, I. Klimant, C. Krause, T. Werner, T. Mayr and O. S. Wolbeis, *Fresenius J. Anal. Chem.*, 2000, **368**, 196.
5 S. M. Borisov, G. Neurauter, C. Schroeder, I. Klimant and O. S. Wolbeis, *Appl. Spectrosc.*, 2006, **60**, 1167–1173.
6 G. S. Vasylevska, S. M. Borisov, C. Krause and O. S. Wolfbeis, *Chem. Mater.*, **18**, 4609–4616.
7 C. Von Bûltzingslöwen, A. K. McEvoy, C. McDonagh and B. MacCraith, *Anal. Chim. Acta*, 2003, **480**, 275–283.
8 G. J. A. A. Soler-Illia, C. Sanchez, B. Lebeau and J. Patarin, *Chem. Rev.*, **102**, 4093–4138.

9 J. S. Beck, J. C. Vartuli, W. J. Roth, M. E. Leonovicz, C. T. Kresge, K. D. Schmitt, C. T. W. Chu, D. H. Olson and E. W. Sheppard, *J. Am. Chem. Soc.*, **114**, 10834–10843.
10 L. Nicole, C. Boissière, D. Grosso, P. Hesemann, J. Moreau and C. Sanchez, *Chem. Commun*.2312–2313.
11 S. A. El-Safty, D. Prabhakaran, A. A. Ismail, H. Matsunaga and F. Mizukami, *Adv. Funct. Mater.*, **17**, 3731–3745.
12 G. Wirnsberger, B. J. Scott and G. D. Stucky, *Chem. Commun*.119–120.
13 F. Hoffmann, M. Cornelius, J. Morell and M. Fröba, *Angew. Chem., Int. Ed.*, **45**, 3216–3251.
14 L. Nicole, C. Boissière, D. Grosso, A. Quach and C. Sanchez, *J. Mater. Chem.*, **15**, 3598–3627.
15 C. Sanchez, C. Boissiere, D. Grosso, C. Laberty and L. Nicole, *Chem. Mater.*, **20**, 682–737.
16 L. L. Li, C. J. Fang, H. Sun and C. H. Yan, *Chem. Mater.*, **20**, 5977–5986.
17 C. Rottman, G. Grader, Y. De Hazan, S. Melchior and D. Avnir, *J. Am. Chem. Soc.*, **121**, 8533–8543.
18 O. B. Miled, C. Sanchez and J. Livage, *J. Mater. Sci.*, **40**, 4523–4530.
19 C. J. Brinker, Y. Lu, A. Sellinger and H. Fan, *Adv. Mater.*, **11**, 579–585.
20 H. Y. Fan, Y. F. Lu, A. Stump, S. T. Reed, T. Baer, R. Schunk, L. V. Perez, G. P. Lopez and C. J. Brinker, *Nature*, 2000, **405**, 56–60.
21 J. B. Pang, J. N. Stuecker, Y. B. Jiang, A. J. Bhakta, E. D. Branson, P. Li, J. Cesarano, D. Sutton, P. Calvert and C. J. Brinker, *Small*, 2008, **4**, 982–989.
22 P. Innocenzi, T. Kidchob, P. Falcaro and M. Takahashi, *Chem. Mater.*, **20**, 607–614.
23 P. D. Yang, G. Wirnsberger, H. C. Huang, S. R. Cordero, M. D. McGehee, B. Scott, T. Deng, G. M. Whitesides, B. F. Chmelka, S. K. Buratto and G. D. Stucky, *Science*, 2000, **287**, 465–467.
24 D. Grosso, C. Boissière, L. Nicole and C. Sanchez, *J. Sol-Gel Sci. Technol.*, **40**, 141–154.
25 M. Etienne, A. Quach, D. Grosso, L. Nicole, C. Sanchez and A. Walcarius, *Chem. Mater.*, **19**, 844–856.
26 P. C. Angelome and G. J. A. A. Soler-Illia, *J. Mater. Chem.*, **15**, 3903–3912.
27 F. H. Dickey, *Proc. Natl. Acad. Sci. U. S. A.*, **35**, 227–229.
28 M. E. Diaz-Garcia and R. B. Laino, *Microchim. Acta*, 2005, **149**, 19–36.
29 E. L. Holthoff and F. V. Bright, *Acc. Chem. Res.*, 2007, **40**, 756–767.
30 R. Gupta and A. Kumar, *Biotechnol. Adv.*, **26**, 533–547.
31 M. J. Whitcombe, M. E. Rodriguez, P. Villar and E. N. Vulfson, *J. Am. Chem. Soc.*, 1995, **117**, 7105.
32 B. Galland, J. Henrard, P. Martin, S. Crunaire, C. Rivron and T.-H. Tran-Thi, *INRS-Hygiène et Sécurité du Travail-1er Trimestre*, 2010, **218**, 45–50.
33 S. Crunaire and T.-H. Tran-Thi, *FR Patent* 2008 0854755.
34 E. J. Cho and F. V. Bright, *Anal. Chim. Acta*, 2002, **470**, 101–110.
35 Y. Tang, Z. Y. Tao, R. M. Bukowski, E. C. Tehan, S. Karri, A. H. Titus and F. V. Bright, *Analyst*, 2006, **131**, 1129–1136.
36 A. S. Kocincova, S. Nagl, S. Arain, C. Krause, S. M. Borisov, M. Arnold and O. S. Wolfbeis, *Biotechnol. Bioeng.*, **100**, 430–438.
37 H. Paolacci, R. Dagnelie, D. Porterat, F. Piuzzi, F. Lepetit and T.-H. Tran-Thi, *Sens. Transducers J.*, 2007, **82**(8), 1423–1430.
38 R. Dagnelie, F. Lepetit, F. Piuzzi, D. Porterat and T. H. Tran-Thi, *Pollut. Atmos.*, 2009, **202**, 179–191.
39 C. M. Rudzinski, A. M. Young and D. G. Nocera, *J. Am. Chem. Soc.*, 2002, **124**(8), 1723–1727.
40 B. J. Melde, B. J. Johnson and P. T. Charles, *Sensors*, 2008, **8**, 5202–5228.
41 S. A. El-Safty, *Adsorption*, 2009, **15**, 227–239.
42 S. A. El-Safty, D. Prabhakaran, Y. Kiyozumi and F. Mizukami, *Adv. Funct. Mater.*, **18**, 1739–1750.
43 T. H. Yang, C. K. Yee, M. L. Amweg, S. Singh, E. L. Kendall, A. M. Dattelbaum, A. P. Shreve, C. J. Brinker and A. N. Parikh, *Nano Lett.*, **7**, 2446–2451.
44 P. Banet, L. Legagneux, P. Hesemann, J. Moreau, L. Nicole, A. Quach, C. Sanchez and T.-H. Tran-Thi, *Sens. Actuators, B*, **130**, 1–8.
45 P. Banet, D. Porterat, F. Lepetit and T.-H. Tran-Thi, *Sens. Transducers J.*, 2007, **83**(9), 1541–1548.
46 C. Chiappe, F. Del Moro and M. Raugi, *Eur. J. Org. Chem.*, 2001, 3501–3510.
47 M. K.-P. Leung, C.-F. Chow and M. H.-W. Lam, *J. Mater. Chem.*, 2001, **11**, 2985–2991.
48 E. L. Shugart, K. Ahsan, M. R. Detty and F. V. Bright, *Anal. Chem.*, 2006, **78**, 3165–3170.
49 J. Homola, S. S. Yee and G. Gauglitz, *Sens. Actuators, B*, **54**, 3–15.
50 J. Homola, *Chem. Rev.*, 2008, **108**, 462–493.
51 S. M. Borisov and O. S. Wolfbeis, *Chem. Rev.*, **108**, 423–461.
52 P. Johnson and T. L. Whateley, *J. Colloid Interface Sci.*, 1971, **37**, 557–563.
53 S. Braun, S. Rappoport, R. Zusman, D. Avnir and M. Ottolenghi, *Mater. Lett.*, 1990, **10**, 1–5.
54 J. Livage, T. Coradin and C. Roux, *J. Phys.: Condens. Matter*, 2001, **13**, R673–R691.
55 D. Avnir, T. Coradin, O. Lev and J. Livage, *J. Mater. Chem.*, 2006, **16**, 1013–1030.
56 P. C. A. Jeronimo, A. N. Araujo, M. Conceicao and B. S. M. Montenegro, *Talanta*, 2007, **72**, 13–27.
57 M. A. Brook, Y. Chen, K. Guo, Z. Zhang and J. D. Brennan, *J. Mater. Chem.*, 2004, **14**, 1469–1479.
58 T. R. Besanger, Y. Zhang and J. D. Brennan, *J. Phys. Chem. B*, 2002, **106**, 10535–10542.
59 T. R. Besanger, Y. Chen, A. K. Deisingh, R. Hodgson, W. Jin, S. Mayer, M. A. Brook and J. D. Brennan, *Anal. Chem.*, 2003, **75**, 2382–2391.
60 R. Gupta and N. K. Chaudhury, *Biosens. Bioelectron.*, 2007, **22**, 2387–2399.
61 S. M. Zakir Hossain, R. E. Luckham, A.-M. Smith, J. M. Lebert, L. M. Davies, R. H. Pelton, C. D. M. Filipe and J. D. Brennan, *Anal. Chem.*, 2008, **81**, 5474–5483.
62 A. M. Dattelbaum, G. A. Baker, J. M. Fox, S. Iyer and J. D. Dattelbaum, *Bioconjugate Chem.*, 2009, **20**, 2381–2384.